# Validation of the Aura Microwave Limb Sounder temperature and geopotential height measurements

M. J. Schwartz,[1] A. Lambert,[1] G. L. Manney,[1,2] W. G. Read,[1] N. J. Livesey,[1] L. Froidevaux,[1] C. O. Ao,[1] P. F. Bernath,[3,4] C. D. Boone,[3] R. E. Cofield,[1] W. H. Daffer,[1] B. J. Drouin,[1] E. J. Fetzer,[1] R. A. Fuller,[1] R. F. Jarnot,[1] J. H. Jiang,[1] Y. B. Jiang,[1] B. W. Knosp,[1] K. Krüger,[5] J.-L. F. Li,[1] M. G. Mlynczak,[6] S. Pawson,[7] J. M. Russell III,[8] M. L. Santee,[1] W. V. Snyder,[1] P. C. Stek,[1] R. P. Thurstans,[1] A. M. Tompkins,[9] P. A. Wagner,[1] K. A. Walker,[3,10] J. W. Waters,[1] and D. L. Wu[1]

Received 11 April 2007; revised 5 November 2007; accepted 27 December 2007; published 2 May 2008.

[1] Global satellite observations of temperature and geopotential height (GPH) from the Microwave Limb Sounder (MLS) on the EOS Aura spacecraft are discussed. The precision, resolution, and accuracy of the data produced by the MLS version 2.2 processing algorithms are quantified, and recommendations for data screening are made. Temperature precision is 1 K or better from 316 hPa to 3.16 hPa, degrading to ~3 K at 0.001 hPa. The vertical resolution is 3 km at 31.6 hPa, degrading to 6 km at 316 hPa and to ~13 km at 0.001 hPa. Comparisons with analyses (Goddard Earth Observing System version 5.0.1 (GEOS-5), European Centre for Medium-range Weather Forecasts (ECMWF), Met Office (MetO)) and other observations (CHAllenging Minisatellite Payload (CHAMP), Atmospheric Infrared Sounder/Advanced Microwave Sounder Unit (AIRS/AMSU), Sounding of the Atmosphere using Broadband Radiometry (SABER), Halogen Occultation Experiment (HALOE), Atmospheric Chemistry Experiment (ACE), radiosondes) indicate that MLS temperature has persistent, pressure-dependent biases which are between −2.5 K and +1 K between 316 hPa and 10 hPa. The 100-hPa MLS v2.2 GPH surface has a bias of ~150 m relative to the GEOS-5 values. These biases are compared to modeled systematic uncertainties. GPH biases relative to correlative measurements generally increase with height owing to an overall cold bias in MLS temperature relative to correlative temperature measurements in the upper stratosphere and mesosphere.

**Citation:** Schwartz, M. J., et al. (2008), Validation of the Aura Microwave Limb Sounder temperature and geopotential height measurements, *J. Geophys. Res.*, *113*, D15S11, doi:10.1029/2007JD008783.

## 1. Introduction

[2] The Microwave Limb Sounder (MLS) [*Waters et al.*, 2006] on the Aura spacecraft [*Schoeberl et al.*, 2006], launched on 15 July 2004, observes thermal microwave limb emission from many molecules, including $O_2$. This paper describes MLS measurements of temperature and geopotential height (GPH) that are produced by version 2.2 of the MLS data processing algorithms (v2.2). The precision and resolution of these measurements are discussed, and accuracy is estimated through comparison with validated correlative data sets and by modeling the impacts of measurement parameter uncertainties.

[3] Knowledge of the thermodynamic state of the atmosphere is fundamental to atmospheric dynamics, chemistry, and radiation. MLS measurements of temperature, GPH and the related assignment of tangent-point pressures (ptan) to individual limb-views are also critical steps in obtaining the atmospheric constituents.

[4] The Microwave Limb Sounder (MLS) on NASA's Earth Observing System (EOS) Aura satellite measures ~3500 vertical profiles per day along the suborbital track. Initial validation of the first publicly available Aura MLS data set, version 1.5 (v1.5), was presented by *Froidevaux et al.* [2006]. Here we report on the quality of the recently released v2.2 temperature and GPH measurements.

[1]Jet Propulsion Laboratory, California Institute of Technology, Pasadena, California, USA.
[2]Department of Physics, New Mexico Institute of Mining and Technology, Socorro, New Mexico, USA.
[3]Department of Chemistry, University of Waterloo, Waterloo, Ontario, Canada.
[4]Now at Department of Chemistry, University of York, York, UK.
[5]Leibniz Institute for Marine Sciences, IFM-GEOMAR, Kiel University, Kiel, Germany.
[6]NASA Langley Research Center, Hampton, Virginia, USA.
[7]Global Modeling and Assimilation Office, NASA Goddard Space Flight Center, Greenbelt, Maryland, USA.
[8]Hampton University, Hampton, Virginia, USA.
[9]European Centre for Medium-range Weather Forecasts, Reading, UK.
[10]Now at Department of Physics, University of Toronto, Toronto, Ontario, Canada.


0148-0227/08/2007JD008783

[5] The v2.2 measurement system is described in section 2. In addition to providing a review of instrumental and orbital characteristics, this section includes guidelines for quality control screening of the v2.2 temperature and GPH products, documents their precision and spatial resolution, and quantifies known systematic error. Section 3 focuses on comparisons of MLS data with analyses and collocated satellite observations of temperature and GPH. Finally, section 4 summarizes all these findings, reports on remaining issues with the validation of these MLS data products, and outlines plans for future versions.

## 2. MLS Temperature and GPH Measurement Description

### 2.1. The MLS Measurement System

[6] MLS observes thermal microwave emission by the atmosphere in five spectral regions from 115 GHz to 2.5 THz. The temperature and GPH measurements described in this paper are taken from observations near the 118-GHz $O_2$ spectral line and the 234-GHz $O^{18}O$ spectral line. MLS looks forward from the Aura spacecraft and scans the Earth's limb vertically from the ground to ~90 km every 24.7 s. The vertical scan rate varies with altitude, with a slower scan providing greater integration time in the lower regions (~0–25 km). The MLS vertical scans are synchronized to the Aura orbit such that vertical scans are made at essentially the same latitudes each orbit, with 240 scans performed per orbit (~3500 scans per day).

[7] The geophysical products described in this paper are retrieved from calibrated MLS limb radiances using MLS version 2.2, level-2 software [*Livesey et al.*, 2006]. Temperature and GPH are reported on 12 levels per decade from 1000–22 hPa, 6 levels per decade from 22–0.1 hPa and 3 levels per decade from 0.1–0.001 hPa. 240 profiles are retrieved per orbit, spaced at 1.5° great circle angle along the suborbital track at an essentially fixed set of latitudes. The MLS v2.2 data quality document [*Livesey et al.*, 2007] gives more information on the format and contents of the MLS data files.

[8] Version 2.2 (v2.2) is the second public release of MLS data and has been used to process the incoming data stream since March 2007. Reprocessing of data collected since MLS became operational in August 2004 is also in progress using the v2.2 algorithms. For this validation effort, 93 days were processed with v2.2 algorithms with an emphasis on days of particular interest for validation of various MLS data products.

### 2.2. MLS Temperature and GPH Measurements

[9] The MLS measurement system [*Livesey et al.*, 2006] uses optimal estimation theory [*Rodgers*, 2000] to retrieve an atmospheric state vector. The initial phase retrieves temperature/GPH/ptan using radiances from the vicinity of $O_2$ spectral lines at 118 GHz and 234 GHz. The state vector contains temperature on 47 pressure levels and GPH on the 100-hPa reference surface. The temperature profile and the single reference GPH level determine the rest of the GPH profile through assumed hydrostatic balance. The state vector also includes the tangent pressures (ptan) of the limb observations, and ptan, temperature and refGPH (GPH at 100 hPa) are interrelated through the instrument scan model and assumed hydrostatic balance, and are simultaneously retrieved.

[10] The retrieval obtains temperature information from both "saturated" (optically thick) and "unsaturated" (optically thin) limb radiances. Saturated radiances are a weighted average of the black-body emission over some layer of the atmosphere, so each radiance provides temperature information about some layer. Unsaturated radiances near pressure-broadened $O_2$ lines provide estimates of limb-tangent pressure from line shape. Pressure as a function of limb-pointing height (from the antenna/spacecraft scan model) determines temperature through assumed hydrostatic balance.

[11] The a priori temperature used in the MLS v2.2 retrieval between the surface and 1 hPa is the GEOS-5 analysis, discussed in section 3.1. At levels above 1 hPa, CIRA86 climatology [*Fleming et al.*, 1990] is used. There is an approximately 5-km layer at 1 hPa over which the two sources of a priori transition smoothly. The assumed a priori temperature precision is piecewise linear in log pressure: 5 K at 1000 hPa, 10 K at 220 hPa and 20 K at 68 hPa and lower pressures. The a priori 100-hPa GPH is 16 km and its precision is 5 km. Assumed a priori precisions are chosen conservatively (loosely) so that a priori information is weighted less heavily than information from measured radiances.

### 2.3. Data Usage Guidelines

[12] In addition to describing file formats and contents, the data quality document [*Livesey et al.*, 2007] also gives detailed instructions on the proper use of MLS data products. Each MLS Level 2 data point is reported with a corresponding precision. If the retrieval does not improve precision by at least a factor of two from its a priori value, then it has failed to extract sufficient additional information from radiances and retrieved values will be significantly influenced by a priori. Such precisions are set negative, and these data are not recommended for use in scientific studies. There is further discussion of temperature and GPH precision in section 2.5.

[13] Three additional data flags are provided for every vertical profile. "Status" is a bit field indicating operational abnormalities or problems with the retrievals. The meanings of its bits are given by *Livesey et al.* [2007]. Profiles for which Status is an odd number should not be used in any scientific study. Nonzero but even values of Status indicate that the profile has been marked as questionable by the data processing software, usually because of possible significant influence by thick clouds. At pressures of 147 hPa and lower (higher in the atmosphere), the cloud bits may generally be ignored. In the troposphere an attempt has been made to screen out radiances that have been influence by clouds, but some cloud-induced negative biases in retrieved temperature of up to 10 K are still evident, particularly in the tropics. The low-cloud bit of Status is meant to flag possible instances of such impacts, but validation work has shown this flag to be lagged 1–2 profiles from the impacted profile. Temperatures in the tropopause (316–178 hPa) should be rejected as possibly influenced by cloud if the low-cloud Status bit (Status AND 32) is set in either of the two profiles following the profile in question.

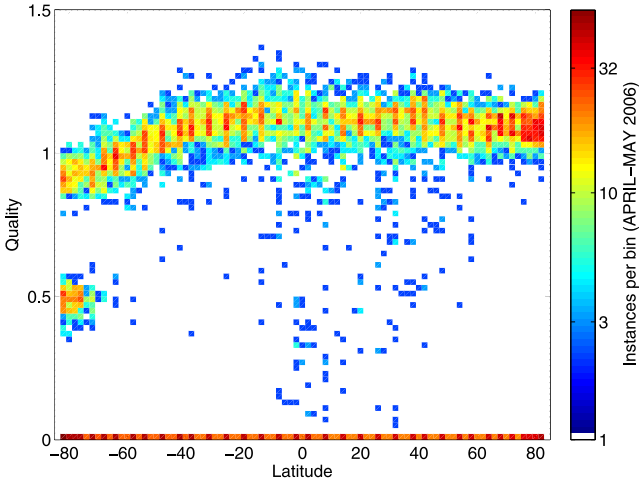


**Figure 1.** Temperature Quality flag for April–May 2006. In the polar autumn, south of 70°S, profiles for which the final phase of the temperature retrieval failed to converge have Quality less than 0.7.

[14] The "Quality" field indicates the degree to which the measured MLS radiances have been fit by the Level 2 algorithms. Larger values of Quality generally indicate better radiance fits, whereas values closer to zero indicate poorer radiance fits, and thus less reliable data. The Quality reported with the v2.2 temperature is based only upon the $\chi^2$ of Band 8 radiances (radiances used in the temperature retrieval are discussed in section 2.4) and so is primarily an indication of the fit of the retrieval in the troposphere. However, low values of Quality are not consistently associated with profiles that are obviously outliers. Profiles having Quality values less than 0.6 are generally not recommended for scientific use. This threshold for Quality typically excludes ~4% of temperature profiles.

[15] The "Convergence" field is a somewhat arbitrarily defined function of $\chi^2$ which can be used to flag profiles within "chunks" of ~10 profiles in which the retrieval failed to converge well. Convergence values around 1.0 typically indicate that the retrieval has converged. Profiles with Convergence greater than 1.2 are not recommended for use in scientific studies. This screening typically rejects 2 percent of profiles, and 0.5 percent in addition to those flagged by Quality <0.6 while flagging most poorly converged profiles.

[16] Temperature and GPH at pressures lower than 0.001 hPa or higher than 316 hPa are not recommended for use in scientific studies. Unlike in v1.5, these levels are not, as a rule, marked with negative precision. An additional cost for departures of the retrieved-profile curvature from a priori curvature has been added to v2.2 to constrain smoothness, as described by *Livesey et al.* [2006]. Neither the degree to which this smoothness constraint leaks a priori information into the retrieval, nor the degree to which it extrapolates retrievals to levels where MLS lacks direct observations, have been properly accounted for in the setting of negative precision in the v2.2 algorithms.

[17] A large set of v2 temperature profiles with low Quality (between 0.4 and 0.55) and high (poor) convergence exists poleward of 70° latitude in autumn and early winter. Figure 1 shows such a cluster of points in data from four days in April and May of 2006, when more than half of profiles south of 70°S had Quality less than 0.6. Here, Quality and Convergence reflect the convergence failure in the final "phase" of the temperature retrieval, which combines radiances from the isotopic $O^{18}O$ line at 234 GHz with radiances from the vicinity of the 118-GHz $O_2$ line. This nonconvergence may be related to poor treatment of $O_3$ in the retrieval. In these cases, the retrieved state falls back to the generally well-behaved output of a previous "phase" that uses only 118-GHz radiances and has somewhat degraded vertical resolution in the troposphere. Biases between the temperatures of the two phases are generally less than 1 K in the stratosphere. For polar stratospheric studies, users may want to relax the Quality threshold to 0.4 to fill in missing data, but the added profiles should not be used at pressures greater than 215 hPa.

[18] In summary, temperature and GPH should be used only when the associated precision is positive, Quality is greater than 0.6, Convergence is less than 1.2, Status is even and the Status low-cloud bit (Status AND 32) is not set in either of the two subsequent profiles. Status low-cloud bits may be ignored at retrieval levels with pressures less than 178 hPa.

### 2.4. Radiance Spectra and Radiance Residuals

[19] Figures 2, 3 (left), and 4 show typical MLS radiances in the vicinity of the 118-GHz $O_2$ line and Figures 3 (right) and 5 show radiances in the vicinity of the $O^{18}O$ line at 234 GHz. Emission in these spectral regions is dominated by oxygen, and is used to infer limb tangent-point pressures of MLS observations and to derive MLS temperature and GPH. The $O_2$ mixing ratio is assumed constant from the surface to 0.008 hPa [*Schwartz et al.*, 2006].

[20] MLS band 22 provides radiances within ±4 MHz of the 118-GHz line center with 100 kHz resolution. Band 1 provides radiances within ±575 MHz of the 118-GHz line center with channel bandwidths ranging from 6 to 96 MHz. Bands 32 and 34 (not shown) have 500-MHz-wide channels centered 1.75 GHz and 3.5 GHz from the 118-GHz line center.

[21] Band 8 has channels within ±575 MHz of the 234-GHz line center with channel bandwidths ranging from 6–96 MHz. Band 33 channel 3 has sidebands with 500-MHz passbands at 232.5 GHz and 246.9 GHz. Radiance precision for this channel is inflated to 1 K to account for systematic uncertainties. This channel is fit to within 0.1 K at the top and bottom of a typical scan, but in the UT/LS it has an average positive residual of 1.5–2 K.

[22] The bottom parts of Figures 2, 3, 4 and 5 show the average fits achieved to these measured radiances by the retrieval algorithms. The scatter about these averages (not shown) is generally consistent with the levels of noise seen in the radiances.

[23] The fits for the saturated channels of Band 1, shown in Figure 2, are generally within ~0.3 K. The outer channels of Band 1, which are used in the midstratosphere and above, have residuals of magnitude 0–1 K, with more variability among channels than is seen in the saturated radiances. Residuals in the unsaturated outer channels have an asymmetry about the line center which is not understood.

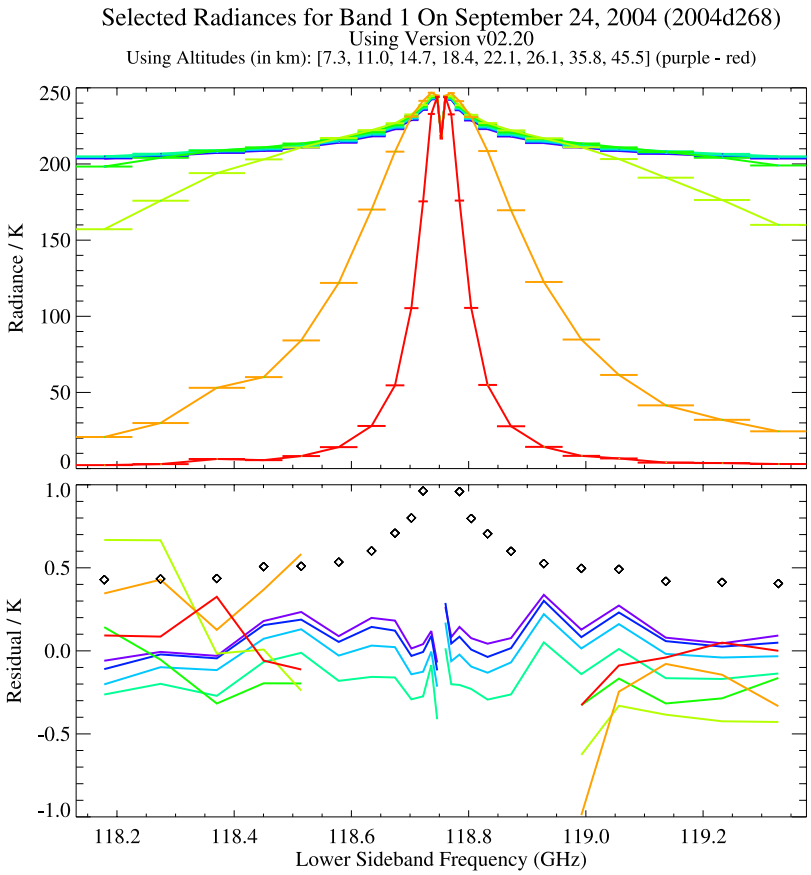


**Figure 2.** (top) Sample radiances (in units of brightness temperature) from MLS Band 1, centered on the 118-GHz $O_2$ line. Global average radiances from observations on 24 September 2004 are shown for eight scan positions with approximate tangent altitudes: ~7.5 km (purple), ~11 km (dark blue), ~15 km (light blue), ~18 km (dark green), ~22 km (light green), ~26 km (yellow green), ~36 km (orange), and ~46 km (red). This is a single-sideband radiometer, so all radiances are from below the 126-GHz local oscillator. These radiances are the primary source of MLS temperature in the stratosphere and lower mesosphere. The widths of the various MLS spectral channels are denoted by the horizontal bars. (bottom) The average fit achieved to these radiances by the MLS v2.2 retrieval algorithms. The v2.2 retrieval does not use channels 6–20 for limb-pointings with tangent pressures less than 50 hPa, so these channels do not have residuals for the four highest altitudes shown. Diamonds are radiance precisions used in the retrieval's $\chi^2$ calculations.

[24] Bands 32 and 34 have 500-MHz wide channels centered 1.75 GHz and 3.25 GHz from the 118-GHz $O_2$ line for horizontal and vertical linear polarizations, respectively, and provide temperature information in the lowermost stratosphere and tropical tropopause layer. Polarization is not significant in these channels, and signals should be approximately symmetric about the line center, so these channels should be essentially quadruply redundant, but the mean residuals in presumably redundant channels differ by as much as 1 K, large compared to the 0.25- to 0.4-K estimated measurement precisions. These residuals are apparently the result of instrumental issues rather than deficiencies in geophysical modeling of radiances. The precisions of these channels have been inflated to 1 K so that the retrieval's $\chi^2$ calculation does not force the retrieved state to closely fit these systematic errors.

[25] Band 22 radiances and residuals are shown in Figure 4. Band 22 radiances cover the line center of the 118 GHz $O_2$ line, which is Zeeman-split by the Earth's magnetic field [*Schwartz et al.*, 2006]. The relative orientation of the Earth's magnetic field to the MLS R1A radiometer's field-of-view and polarization results in a pair of Zeeman components being received by Band 22 for most parts of an orbit. These radiances contribute to the temperature retrieval primarily in the mesosphere and lower thermosphere (~0.1–0.001 hPa). The blue lines show radiances and residuals for a pointing with an average tangent height of ~60 km (~0.22 hPa,) where the radiance is just starting to come out of saturation at the band edges. Residuals at this level are as large as 3–4 K in the band edges, and the inability of the retrieval to fit these radiances better may, in part, result from gain compression, which distorts spectral line shapes, as is discussed in section 2.6. Unlike in the case of Band 1 radiances, Band 22 radiances are used from where they are saturated to where they are optically thin. Residuals in the highest pointings shown (~81 km: yellow, ~93 km: red) display a line shift due to some combination of error in the Doppler-shift correction

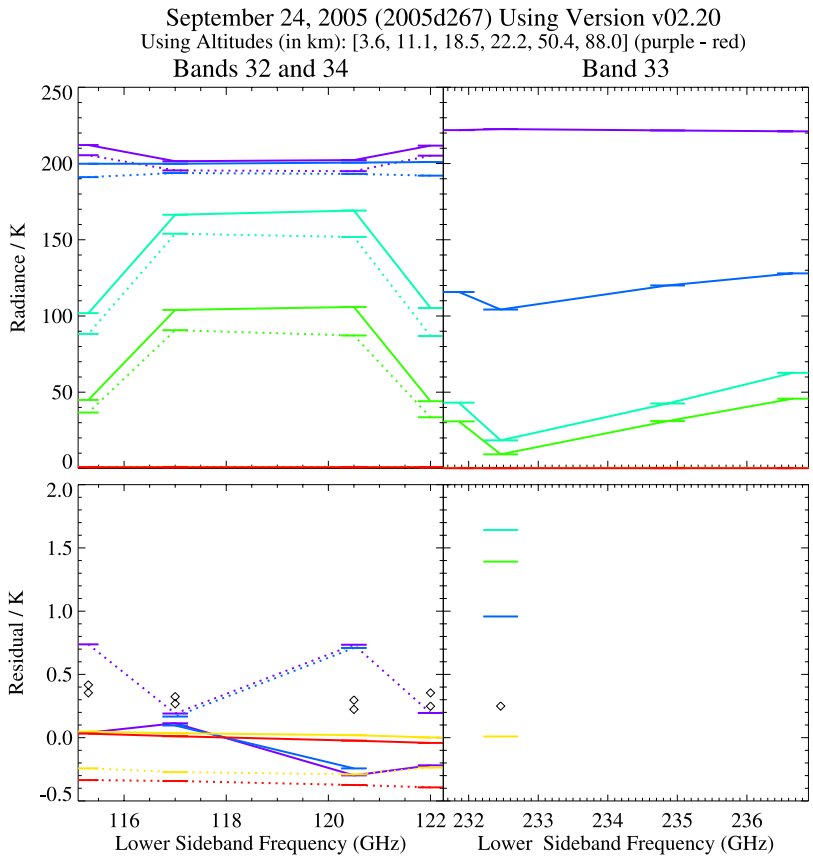


**Figure 3.** As in Figure 2, except for Band 32 (solid line) and Band 34 (dashed line) overlaid on left and Band 33 overlaid on the right. Radiances are shown for six scan positions with approximate tangent altitudes: 3.5 km (purple), 11 km (blue), 18.4 km (dark green), 22 km (light green), 50 km (yellow), and 87.9 km (red). Diamonds on bottom plots show theoretical precisions based upon radiometer noise and channel bandwidth, but these channel precisions are inflated to 1 K in $\chi^2$ calculations of the retrieval to account for systematic uncertainties.

for spacecraft-Earth relative motion and unmodeled mesospheric along-track wind, and provide an opportunity for along-track wind retrieval [e.g., *Limpasuvan et al.* 2005].

### 2.5. Precision, Scatter, and Spatial Resolution

[26] Each point in an MLS retrieved profile is accompanied by a "precision" estimate taken from the diagonal of the solution covariance matrix [*Livesey et al.*, 2006]. Precision quantifies random error, expected to beat down when repeated measurements are averaged, which results from the propagation of radiometric noise and of uncertainties in virtual measurements through the measurement system. Temperature precisions range from 0.6 K in the lower stratosphere to 2.5 K in the mesosphere and to 1 K at 316 hPa. In this discussion "precision" is distinguished from "accuracy," which is the RMS of the difference from truth. Accuracy is estimated through analysis of sources of systematic error (discussed in section 2.6) and through comparisons with correlative measurements (section 3).

[27] Differences between repeated measurements of similar scenes provide an empirical upper bound on precision which can be compared to the precision returned by the retrieval system. Successive profiles generally see very similar scenes but have correlation due to shared calibration data, so their difference gives an unrealistically low value for precision. Profiles exactly one orbit apart are at the same latitude and local time, separated by 21 degrees of longitude, and may provide a useful upper bound on precision when the atmosphere is zonally symmetric. Precision estimates based upon such pairs in high-latitude summer are slightly larger than those returned by the measurement system in the troposphere and lower stratosphere and a factor of ~1.4 larger from the middle stratosphere through the mesosphere.

[28] Poleward of 70°S on 7 February 2005, precision inferred from differences between successive orbits is 1.5 K at 316 hPa, 1 K or less from 100 hPa to 10 hPa, 1.4 K at 1 hPa, 2.3 K at 0.1 hPa, 3 K at 0.01 hPa and 3.5 K at 0.001 hPa. Tropical orbital crossings from the same day (within 50 km in distance but 12 hours different in local time) have RMS differences of 1 K at 316 hPa, providing an even lower limit on precision at this level.

[29] As the 100-hPa level is the only GPH element in the state vector, GPH precision is calculated at other levels by adding the contributions of this reference level precision and the temperature profile precisions, in quadrature. The resulting GPH precision profile always has a minimum value at the reference level, a nonphysical result of the neglect of off-diagonal elements in the solution's error covariance.

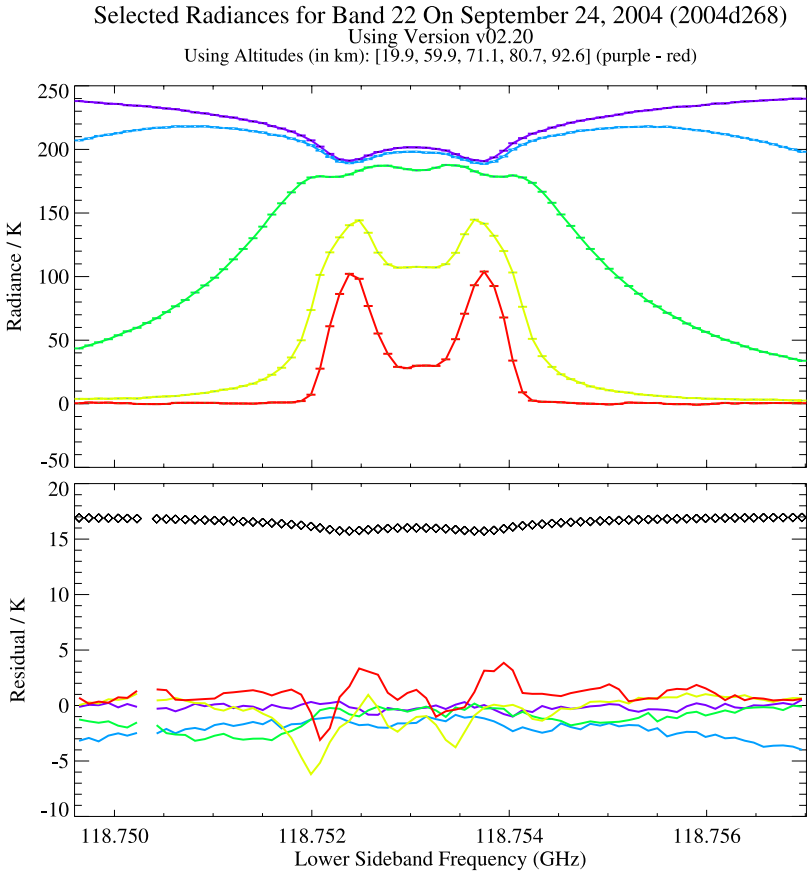


**Figure 4.** As in Figure 2. Band 22 radiances cover the opaque line center of the 118.75-GHz $O_2$ line, which is Zeeman-split by the Earth's magnetic field. Radiances are shown for five scan positions with approximate tangent altitudes: 20 km (purple), 60 km (blue), 71 km (green), 81 km (yellow-green), and 93 km (red).

[30] The 100 hPa level is, in fact, close to the level where line width information provides the best pointing/pressure reference and the overestimate of GPH precision at other levels is expected to be of order 10 m or less. Calculated GPH precisions, given in column 7 of Table 1, are ~35 m from 316 hPa to 100 hPa, 44 m at 1 hPa, 110 m at 0.001 hPa.

[31] The MLS retrieval algorithms operate in a two dimensional, tomographic manner [*Livesey and Read*, 2000; *Livesey et al.*, 2006] that permits the direct modeling of line-of-sight gradients. Two dimensional averaging kernels [*Rodgers*, 2000] describe both vertical and horizontal resolution. Figure 6 shows the vertical temperature averaging kernels which result from the horizontal integration of the 2-D kernels. The vertical resolution of the MLS temperature measurement, taken to be the full width at half maximum of these averaging kernels, is 5.3 km at 316 hPa, 5 km at 100 hPa, 3.5 km at 32 hPa, 4 km at 10 hPa, 8 km at 1 hPa, 9 km at 0.1 hPa, 14 km at 0.01 hPa and 15 km at 0.001 hPa. In the along-track horizontal direction (not shown), the temperature data have single profile resolution (~165 km) through most of the profile, degrading to 185 km at 0.01 hPa and to 220 km at 0.001 hPa. The cross-track horizontal resolution is defined by the horizontal width of the MLS field of view. For the 240-GHz radiometer, which provides information in the troposphere, this width is ~6 km, and for the 118-GHz radiometer, which provides information from the tropopause upward, it is ~12 km.

### 2.6. Accuracy and Systematic Error Budgets

[32] Systematic uncertainties arise from instrumental issues (e.g., radiometric calibration, field of view characterization), spectroscopic uncertainty, and approximations in the retrieval formulation and implementation. This section summarizes the relevant results of a comprehensive quantification of these uncertainties that was performed for all MLS products. More information on this assessment is given in Appendix A of *Read et al.* [2007].

[33] For each identified source of systematic uncertainty, the impact of a 2-$\sigma$ perturbation of the relevant parameter upon MLS measured radiance and/or pointing has been estimated. For primary sources of systematic uncertainty, a full day of simulated, cloud-free radiances is generated for each perturbation, and these perturbed measurements are run through the routine MLS v2.2 processing algorithms. Comparison of these results with those of a retrieval on unperturbed radiances identifies both resulting systematic bias and scaling as well as additional scatter in the retrieval results. The extent to which scatter can be expected to average down is estimated to first order by these "full up

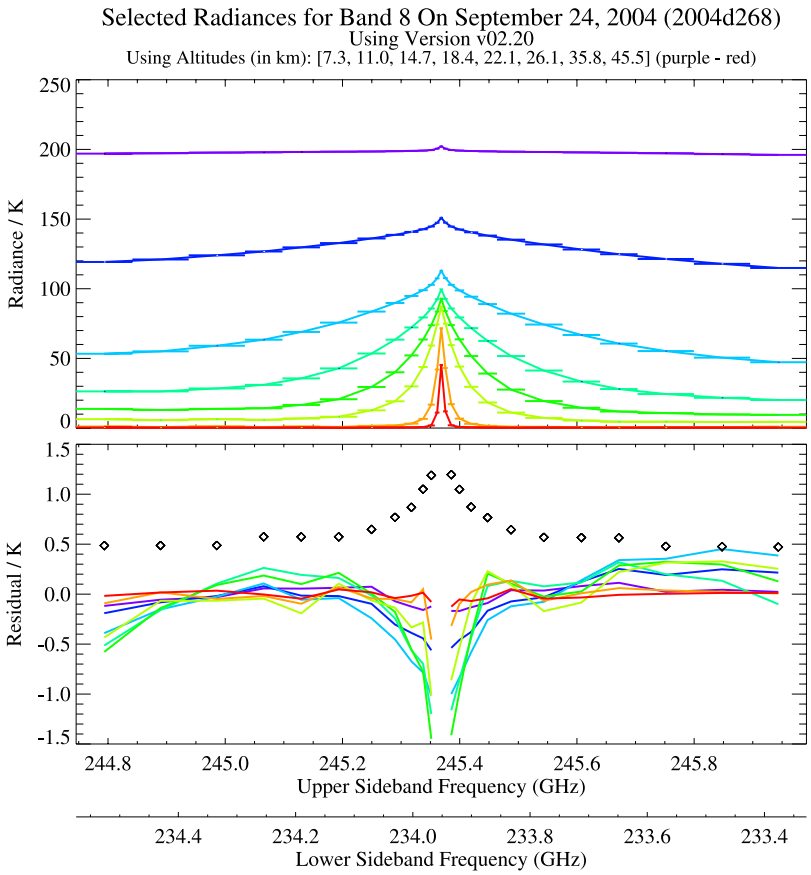


**Figure 5.** As in Figure 2, except for Band 8. Radiances are global averages from 24 September 2004 for eight scan positions with approximate tangent altitudes: 7.3 km (purple), 11 km (dark blue), 14.7 km (light blue), 18.4 km (dark green), 22 km (green), 26 km (yellow green), 35 km (orange), and 45.5 km (red).

studies" through their separate consideration of the bias and scatter each source of uncertainty introduces into the data.

[34] The difference between the retrieved product in the unperturbed run and the original "truth" model atmosphere is taken as a measure of uncertainties due to retrieval formulation and numerics. Another retrieval of the unperturbed radiances is performed with 3 K added to the temperature a priori to test sensitivity to its value.

[35] The impact of an additional set of minor systematic uncertainties has been estimated through calculations based on simplified models of the MLS measurement system *Read et al.* [2007]. Unlike the "full up studies", these calculations only provide estimates of gain uncertainty (i.e., possible multiplicative error) introduced by the source in question.

[36] Figures 7, 8, 9 and 10 summarize the results of this quantification for temperature and GPH. These show the magnitudes of expected biases and additional scatter the various errors may introduce into the data, and should be interpreted as 2-$\sigma$ estimates of their likely magnitude.

[37] Recent laboratory work by the MLS instrument team in estimating the impact of amplifier nonlinearity finds that observed spectrally contrasting signals are "compressed" by $\sim$1.5 percent when viewed against a background scene of 300 K rather than against a scene close to 0 K. The magnitude of this distortion was not recognized until late in the development of version 2.2 algorithms, so there has been no attempt to correct for its impact on retrievals. Of the sources of systematic uncertainty considered in this work, gain compression makes the largest contributions to both temperature and GPH biases, and both the magnitude and sign of the resulting biases can be estimated. Other sources of bias have been modeled by propagating the uncertainty in some parameter (e.g., radiometer pointing offset) through the retrieval system, and the signs of the resulting errors are unknown. The impact of gain compression on retrieved temperature and on GPH is shown in Figures 8 and 10, respectively. Gain compression causes vertical oscillations in MLS v2.2 retrieved temperatures between 316 hPa and 10 hPa which are strikingly similar to those seen in comparisons with correlative data in section 3. However, modeled gain compression also causes a 1–3 K high bias at levels above 10 hPa, while comparisons with correlative data generally suggest that MLS has a low bias at these levels. Thus, initial estimates are that correction for gain compression in a future version of the MLS retrieval will improve agreement with correlative measurements at lower retrieval levels but make it worse at higher levels.

[38] The contribution of cloud effects to the systematic uncertainty, both from the presence of clouds not thick enough to be screened out by the cloud filtering and from the loss of information through omission of cloud-impacted radiances, has been quantified by adding scattering from a representative cloud field to the simulated radiances and

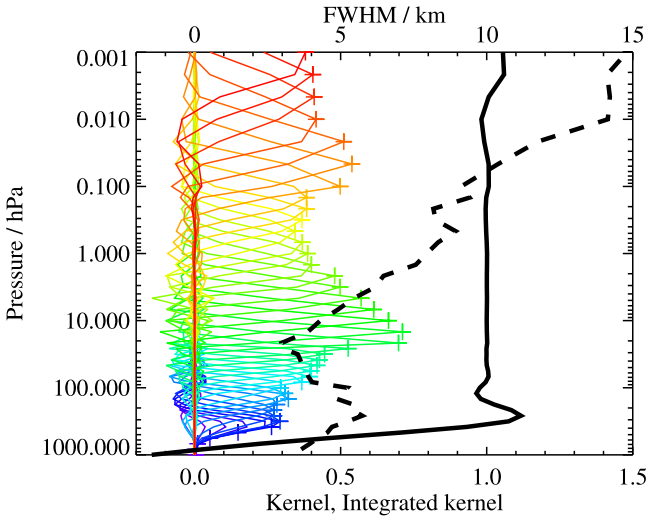


**Figure 6.** MLS v2.2 temperature vertical averaging kernels resulting from horizontal, along-track integration of 2-D averaging kernels for 35°N, September climatology. Individual colored lines show the contribution of atmospheric temperatures at each level to a given MLS retrieved temperature, with the retrieval level marked by a plus sign of the same color. The full width at half maximum (vertical resolution, in kilometers) is shown by the thick black dashed line. The solid black line shows the integrated area under the kernels as a function of MLS retrieval level. Where the integrated area is close to unity, the majority of the information comes from the atmosphere. Lower values are associated with increased contributions from a priori information.

comparing retrievals based on these radiances to the unperturbed results. The cloud-induced effects on temperature shown in Figure 7 are estimated by considering only the cloudy profiles (as defined by the known amount of cloud in the "truth" field). Cloud is estimated here to contribute 0.2 K or less to temperature bias at 100 hPa, increasing to ~1.5 K with a ~3.5 K standard deviation at 316 hPa.

[39] The largest contributions to systematic temperature uncertainty, apart from gain compression, are from "radiometric/spectroscopic" sources and "spectroscopy/forward model" sources, shown in cyan and green, respectively, on Figure 7. The forward model contributes a bias uncertainty of ~3 K in the upper troposphere where temperature information is primarily supplied by unsaturated radiances from Band 8, as discussed in section 2.4. Uncertainty in the $O_2$ line width parameter results in systematic bias uncertainty of 0.5 K or less in the lower stratosphere and of 1 K or less in the troposphere. The contributions of antenna transmission and field-of-view shape uncertainties (the magenta line on Figure 7) are a ~0.5 K systematic uncertainty bias which is nearly uniform with retrieval level. Their contribution to scatter is less than 0.3 K.

[40] Over the range (316–0.001 hPa) of retrieval levels recommended for scientific use, this study indicates a bias uncertainty of up to 2–2.5 K between 100 hPa and 0.01 hPa, of up to 5 K at 316 hPa, and up to 3 K at 0.001 hPa. Additionally, gain compression contributes a generally positive bias to temperature between −2 K and 5 K with oscillatory vertical structure. The aggregate contribution to scatter is ~1 K between 100 hPa and 0.01 hPa, increasing to ~4 K between 100 hPa and 316 hPa and to ~3 K between 0.01 hPa and 0.001 hPa.

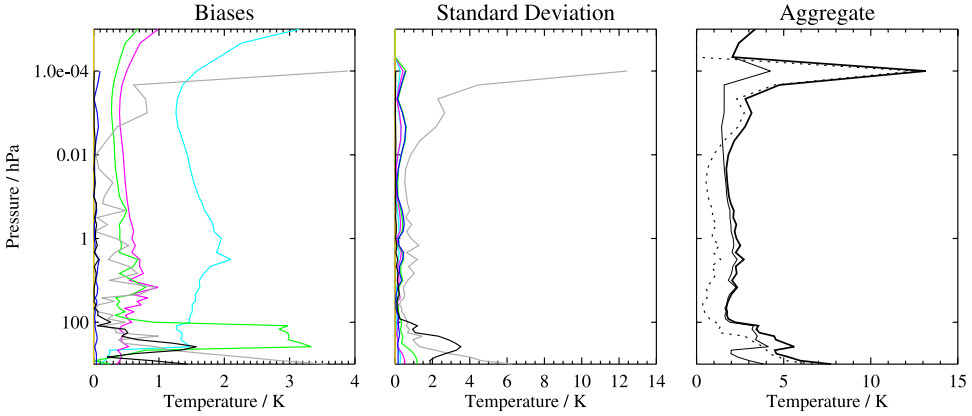


**Figure 7.** The estimated impact of various families of systematic uncertainties on the MLS temperature observations. (left) Magnitude of possible biases of unknown sign and (middle) additional scatter introduced by the various families of errors, with each family denoted by a different colored line. Cyan lines denote errors in MLS radiometric and spectral calibration. Magenta lines show errors associated with the MLS field of view and antenna transmission efficiency. Red lines depict errors associated with MLS pointing uncertainty. The impact of possible errors in spectroscopic databases and forward model approximations are denoted by the green line, and the combined effect of error in retrieval numerics and sensitivity to a priori is shown in grey. The blue lines show the impact of similar "knock on" errors in other species. Finally, the typical impact of cloud contamination is denoted by the purple line. (right) The root sum squares (RSS) of all the possible biases (thin solid line), all the additional scatters (thin dotted line), and the RSS sum of the two (thick solid line).

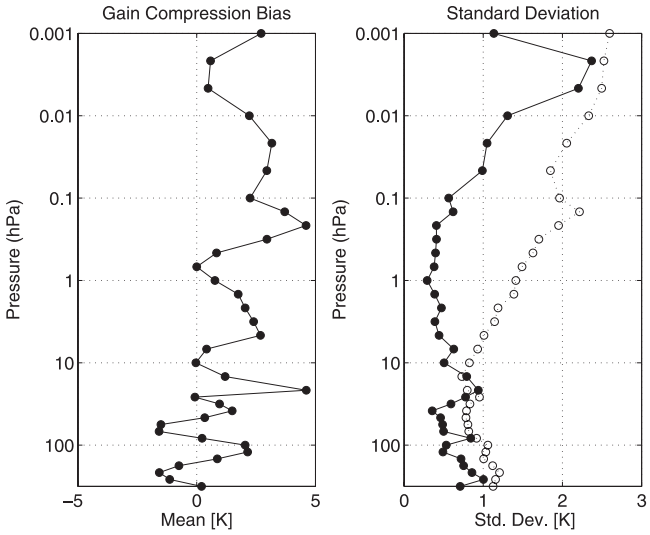


**Figure 8.** The modeled contribution of gain compression to systematic temperature error. Gain compression distorts spectral features, making temperature inferred from line-width-based pressure measurements and hydrostatic balance inconsistent with those made from saturated radiances. (left) The mean difference between profiles retrieved from simulated radiances with and without gain compression. (right) Closed circles are the RMS scatter in the difference between the two retrievals. Open circles are the precision of the single-profile difference.

[41] Systematic uncertainty of GPH can be broken into uncertainties that affect GPH on the 100-hPa reference level, and those that affect GPH profiles through retrieved temperature uncertainties. The contribution of gain compression, shown in Figure 8, results in a positive bias of ~140 m in the 100-hPa reference GPH as well as an increasingly positive bias with height. Other sources of systematic uncertainty contribute on the order of 150 m of bias of unknown sign. The largest terms are due to uncertainty in the $O_2$ line width (~100 m) and uncertainty in the 118-GHz radiometer field-of-view pointing offset from the 240-GHz radiometer (~100 m,) both of which are components of "pointing" on Figure 9. Retrieval numerics contribute up to 100 m of bias and up to 250 m of scatter in mesospheric GPH.

### 2.7. Comparison of v2.2 and v1.5 Temperature and GPH Data

[42] This paper describes temperature and GPH produced by v2.2 of the MLS data processing algorithms. The previous publicly released MLS data product, v1.5, has been produced for 95 percent of the days from August 15, 2004 to the end of February 2007. Both v1.5 and v2.2 use radiances from MLS Bands 22, 1, and 32/34, centered on the 118.75 GHz $O_2$ line and described in section 2.4. V2.2 also uses radiances from MLS Band 8 and Band 33 channel 3 near the isotopic $O^{18}O$ line at 236 GHz to improve resolution in the troposphere. V2.2 temperature, GPH and water vapor are retrieved on a higher-resolution grid in the troposphere and lower stratosphere, with 12 levels per decade from 1000 to 22 hPa rather than the six levels per decade of v1.5. The MLS v2.2 temperature retrieval uses GEOS-5 temperature (discussed in section 3.1) as its a priori while v1.5 used GEOS-4 [*Bloom et al.*, 2005].

[43] Figure 11 shows the mean difference between MLS v2.2 and MLS v1.5 temperature profiles from the first 93 days selected for processing with v2.2 algorithms. V2.2 has a ~2.5-K cold bias relative to v1.5 throughout the stratosphere and mesosphere, and an additional ±2 K of persistent vertical oscillation. The exclusion of unsaturated radiances in the center of Band 1 in v2.2 retrievals changes the net effect of gain compression (discussed in section 2.6) on retrieved temperature, and is believed to be the main cause of bias between versions.

[44] Once reprocessing of the first 30 months of the mission is complete, v2.2 temperature will generally be preferred over v1.5 for scientific studies. Both retrieval versions have biases. V2.2 has slightly better vertical resolution in the upper troposphere, although somewhat poorer vertical resolution in the upper stratosphere. V2.2 has been more extensively validated and is consistent with the improved suite of v2.2 standard products. Routine processing of MLS with v1.5 algorithms was discontinued after February, 2007.

[45] Figure 12 shows the difference between v2.2 and v1.5 retrieved GPH, averaged for the same 93-day period. The difference in GPH retrieved by the two versions is

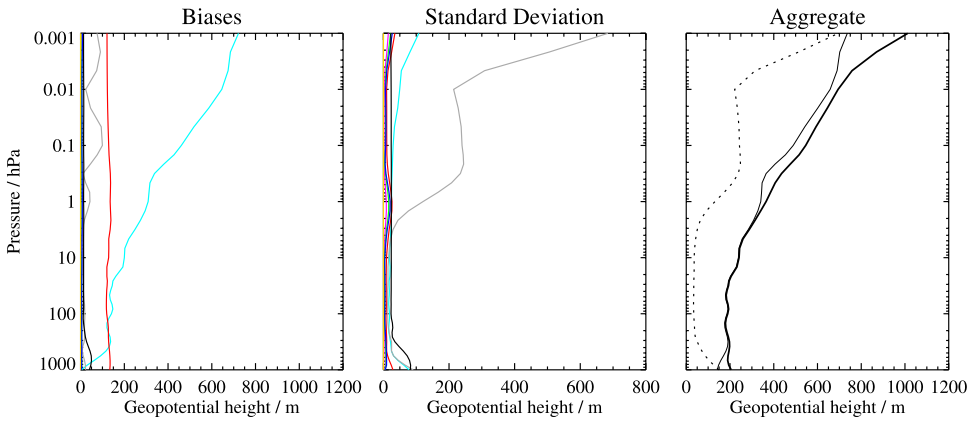


**Figure 9.** The estimated impact of various families of systematic errors on the MLS GPH observations. The description of the lines is the same as in Figure 7 for temperature.

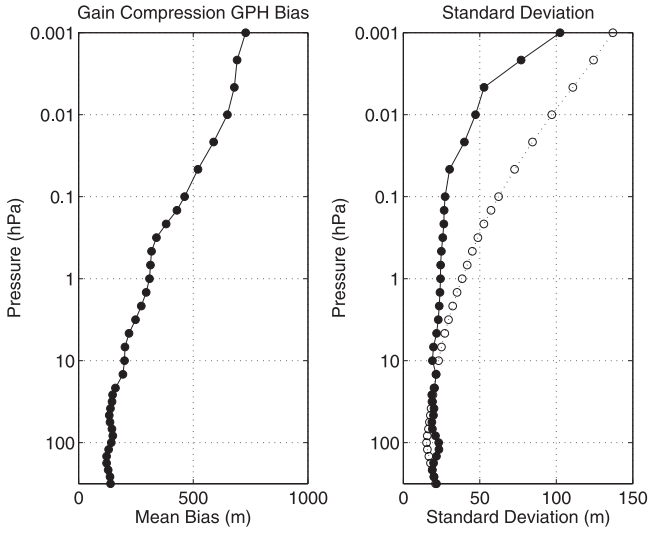


**Figure 10.** The modeled systematic error in GPH due to "gain compression." Plots are as in Figure 8. Gain compression has the largest magnitude contribution to systematic error of any effect considered, and, unlike the others shown in Figure 9, the sign of this bias is significant. A retrieval run on simulated radiances with modeled gain compression matching best current estimates has a high bias in GPH at 100 hPa of ∼140 m compared to the control run, which is similar to the observed bias between MLS and GEOS-5 GPH.

smallest at 100 hPa (0 ± 40 m), but the cold bias in v2.2 relative to v1.5 temperature results in a GPH low bias in v2.2 relative to v1.5 that reaches −600 m at 0.01 hPa. As shown in Figure 9, absolute accuracy of 100 hPa is limited by MLS absolute pointing accuracy, and by the effects of gain compression, and is expected to be poorer than 200 m for both versions. The use of GEOS-5 100 hPa GPH rather than climatology as a priori, along with a tighter a priori precision, would improve this accuracy, but at the possible cost of some geophysical information.

## 3. Comparisons With Other Data Sources

[46] In comparisons with profiles observed by other satellites or from radiosondes, matched pairs of profiles that are closely collocated in space and time are used. The coincidence criteria used to select the matches vary and are stated in each subsection below. Comparison of MLS temperature to radiosondes from the global radiosonde network [*Durre et al.*, 2004] has been not been emphasized in this study, as both GEOS-5 and ECMWF analyses assimilate the radiosonde measurements. A global mean difference and scatter about the mean for 12151 MLS/radiosonde network pairs, coincident within 3 hours and 2 degrees of great circle, is included in the summary plot, Figure 26. The bias is very similar to what is seen with the analyses.

[47] In making these comparisons, it is important to bear in mind that MLS products are not estimates of layer means, rather they are tie points of piecewise-linear profiles in log pressure that are fitted to the observed radiances [*Read et al.*, 2006]. Accordingly, the most appropriate manner to compare MLS retrievals to high-vertical-resolution correlative measurements is to find the piecewise linear fit of the MLS log-pressure grid that best fits the correlative data, and take its grid points [*Livesey et al.*, 2006]. Horizontal piecewise-linear interpolation is neglected owing to the sharpness of the MLS horizontal averaging kernels and the lack of high-horizontal-resolution correlative data.

[48] When evaluating the degree to which a high-vertical-resolution data set is consistent with MLS observations, convolution with MLS averaging kernels may also be needed. Fundamentally, the MLS measurement system retrieves differences from its a priori, which, for MLS v2.2 temperature, is GEOS-5 below 1 hPa and CIRA86 climatology above. When degrading a high-resolution correlative data set to check consistency with MLS observations, it is the difference between the correlative data set and a priori that is convolved with the MLS averaging kernels. Thus the MLS view of sharp features in a correlative data set's vertical temperature profile is degraded by its averaging kernel, but sharp features in the a priori may be passed into the MLS output state.

### 3.1. GEOS-5 Analysis

[49] The GEOS-5 data assimilation system [*Rienecker et al.*, 2007] is a three-dimensional variational (3D-Var) system, combining observations in six-hour windows with six-hour general circulation model (GCM) forecasts. The incremental analysis update (IAU) approach [*Bloom et al.*, 1996] is used in the interface between the observations and the GCM to avoid shocking the model, thus producing smoother analyses. The GCM includes the finite-volume

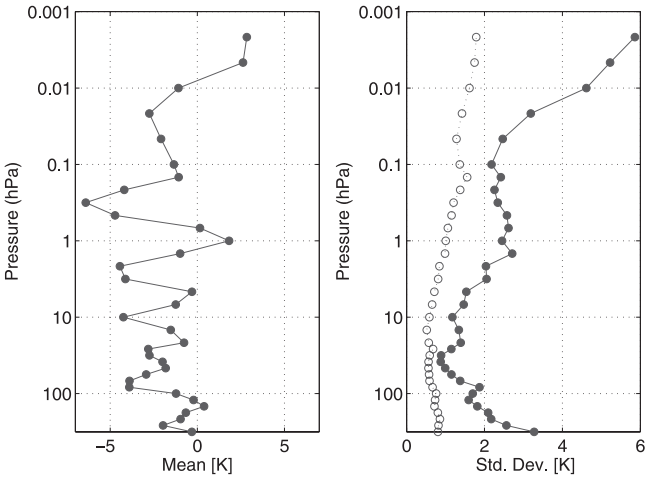


**Figure 11.** MLS v2.2 temperature minus v1.5 temperature, globally averaged for 93 days (287,000 profiles). (left) The mean difference between v2.2 and v1.5. V2.2 has a general ∼2.5-K cold bias relative to v1.5 throughout the stratosphere and mesosphere, with an additional ±2 K of vertical oscillation. Latitudinal variation (not shown) is small compared to persistent vertical structure shown. (right) Solid dots are the 1-$\sigma$ scatter in individual pairs of profiles, and open dots are the average combined estimated individual profile precisions from the two retrievals. MLS v1.5 has been linearly interpolated to the higher-resolution pressure grid of v2.2 in the UTLS.

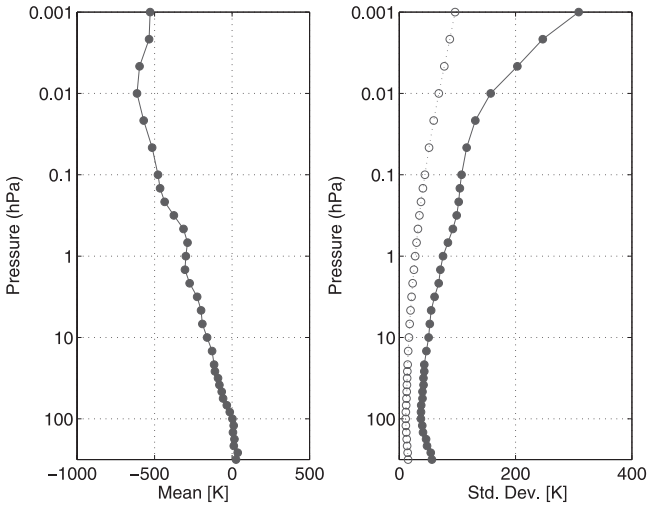


**Figure 12.** MLS v2.2 GPH minus MLS v1.5 GPH, averaged for the first 93 days of v2.2 processing. The plots are as in Figure 11. The two versions agree at 100 hPa to within a 1-$\sigma$ scatter of 40 m, which reflects their use of the same pointing information. The relative temperature bias integrates into a negative bias of v2.2 relative to v1.5 that reaches 600 m at 0.01 hPa.

transport code of *Lin* [2004] along with a package of physical parameterizations. The configuration selected for this work was a 72-layer system with an upper level at 0.01 hPa; the layers transition from terrain-following coordinates in the lowermost troposphere to a pressure system near 186 hPa. A uniform horizontal grid of 0.66° longitude by 0.5° latitude was used. The assimilation is performed using the Grid point Statistical Interpolation (GSI) code of *Wu et al.* [2002]. GSI provides analyses for surface pressure, temperature, winds, moisture and ozone. Observations used to constrain the meteorology include the radiosonde network, infrared radiances from the High-Resolution Spectrometer (HIRS) and the Atmospheric Infrared Sounder (AIRS) on EOS-Aqua, and microwave radiances from the Advanced Microwave Sounding Units on NOAA-15 and NOAA-16. *Stajner et al.* [2007] describe screening and quality control for these observations.

[50] Figure 13 shows 93 days of MLS minus a priori (GEOS-5) temperature averaged for each of the 120 ascending latitudes of an MLS orbit. Artifacts associated with 10-profile "chunk" boundaries are apparent in the mean differences, particularly in the troposphere. At 261 hPa, these artifacts are as large as 1 K. Latitudinal variability is very similar between the hemispheres, and between the ascending and descending portions of the orbits. Vertically oscillating biases are on the order of 1–3 K, while latitudinal variability is typically 1 K. In the tropics at 147–68 hPa, MLS is cooler by ~1 K compared to GEOS-5 than it is at higher latitudes. At 46 hPa and 38 hPa, the pattern is reversed, with ~0.6-K positive biases in the tropics compared to those at higher latitudes.

[51] Variability within the bins is shown in Figure 13 (right). The 1-$\sigma$ scatter about the mean is ~1 K in the lower stratosphere, increasing to ~1.5 K in the troposphere. In the middle stratosphere, midlatitudes have 1.5-K scatter while equatorial and polar bins have variability of 1.5–2.5 K.

[52] Figure 14 shows the difference between MLS retrieved and a priori temperatures for 28 January 2005. The a priori temperature is GEOS-5 for levels below the 1 hPa surface and transitions over 5 km to CIRA86 climatology above. Selected levels from 316 hPa (~9 km) to 0.001 hPa (~91 km) are shown. Profiles marked as possibly influenced by cloud are shown in red, and have outliers of as much as 10 K at the lowest recommended retrieval levels, 316–215 hPa. Those for which Quality was less than 0.6 are shown in green.

[53] Figure 15 shows zonal mean curtain plots of the difference between MLS and GEOS-5 temperatures for months DJF and SON. On these plots, GEOS-5 is used to 0.15 hPa, and it is not replaced by CIRA86 climatology as it is in the MLS a priori. There are persistent vertical oscillations between 316 hPa and 10 hPa with peak-to-peak magnitude ~4 K and latitudinal variation of ~1 K. Northern winter and southern winter (not shown) are similar. MLS is ~10 K warmer than GEOS-5 at 1 hPa in the winter pole, and in both poles near equinox.

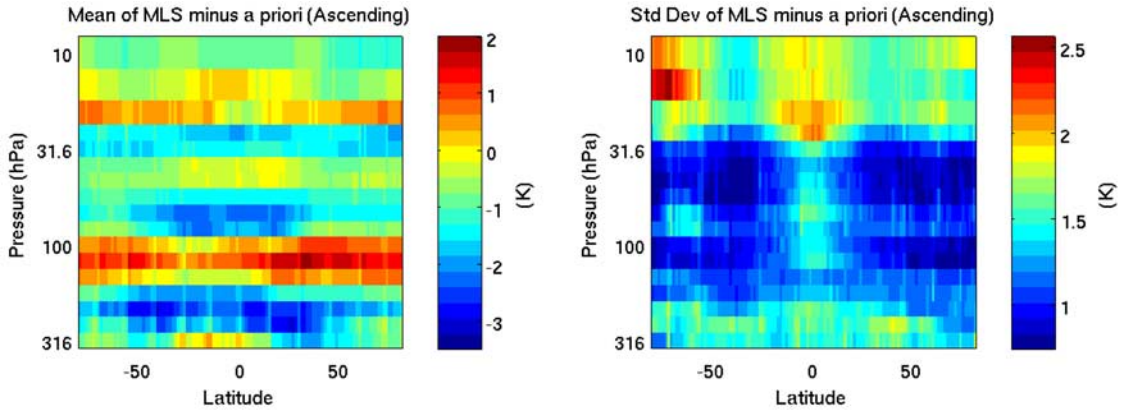


**Figure 13.** MLS minus a priori (GEOS-5) temperature and variability averaged by profile number in orbit, from 316 hPa to 10 hPa. Data are from 93 days processed with v2.2 algorithms and have been averaged for each of the 240 different 1.5° positions around an MLS orbit. The means and standard deviations from the ascending portion of the orbits are shown. Descending portions are similar.

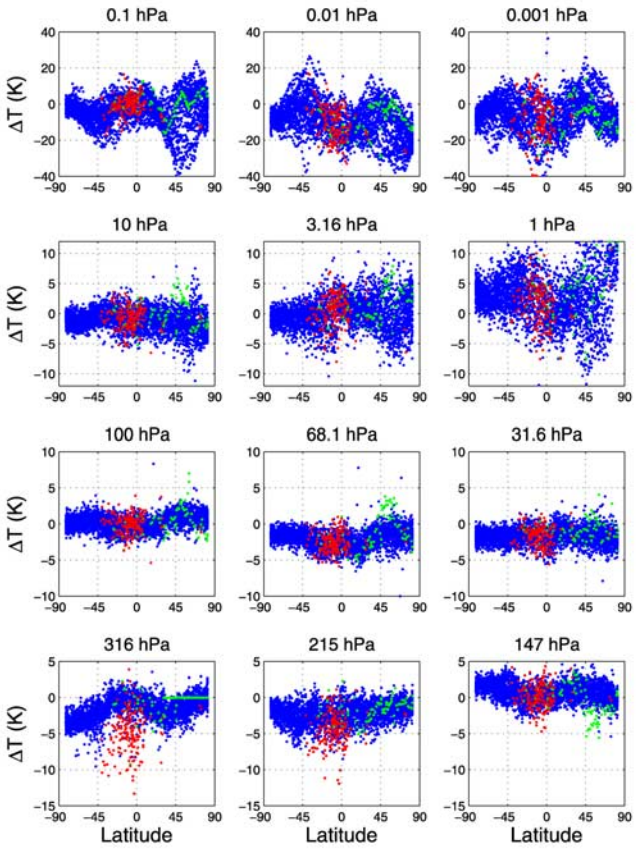


**Figure 14.** MLS v2.2 temperature minus retrieval a priori, for 28 January 2005. Green points have Quality <0.6, and red points are flagged as possibly influenced by cloud using the method recommended in section 2.3. Note the temperature scale changes between plots.

[54] Figure 16 shows seasonally averaged, zonal mean differences between MLS and a priori temperatures. In the upper troposphere and lower stratosphere (316–10 hPa), where GEOS-5 is well supported by assimilated data, systematic biases are evident in the differences which are largely independent of season and latitude. At pressures below 1 hPa, where a priori is CIRA86 climatology, mean differences exceed 10 K at some levels and seasons. Scatter in the differences, shown in Figure 16 (bottom), exceeds 15 K in the northern winter polar mesosphere, where comparison is with climatology.

### 3.2. ECMWF Analysis

[55] The European Center for Medium-range Weather Forecasts (ECMWF) assimilation is a 4D-Variational system based on a spectral GCM [e.g., *Simmons et al.*, 2005]. Operational ECMWF data used here are from two versions of the model. Prior to 1 February 2006, the operational data are from a T511/60-level model with a top at 60 km; after that time, the operational data are from a T799/91-level system with a top at 80 km. Further information on the high-resolution model is given by *Miller and Untch* [2005]. Changes to the ECMWF operational system are documented in the ECMWF newsletters, available at http://www.ecmwf.int/publications/newsletters/. Inputs to the ECMWF assimilation system are very similar to those listed for GEOS-5, including assimilation of AIRS radiances. Data from the T799/91-level model were made available beginning in October 2005, when a model experiment was running, but not operational. Model level data from the T799/91-level system are used at levels up to 0.1 hPa for profile comparisons. The T799/91-level data were extracted on a 2.5° × 2.5° horizontal grid prior to interpolation to the MLS observation points. Figure 17 includes some ECMWF data interpolated to MLS locations from a 1° × 1° grid and some from a 2.5° × 2.5° grid. This difference in horizontal resolution of the grid on which data were extracted from the ECMWF analysis does not have a significant impact on the mean or scatters shown in Figure 17. Synoptic comparisons shown in sections 3.8 and 3.9 use the T511/60-level analyses after interpolation to a 0.5° × 0.5° grid and to standard pressure levels.

[56] Coincident profiles with MLS are constructed by interpolating the 6-hour ECMWF analyses in space and time to MLS observations. ECMWF vertical resolution is

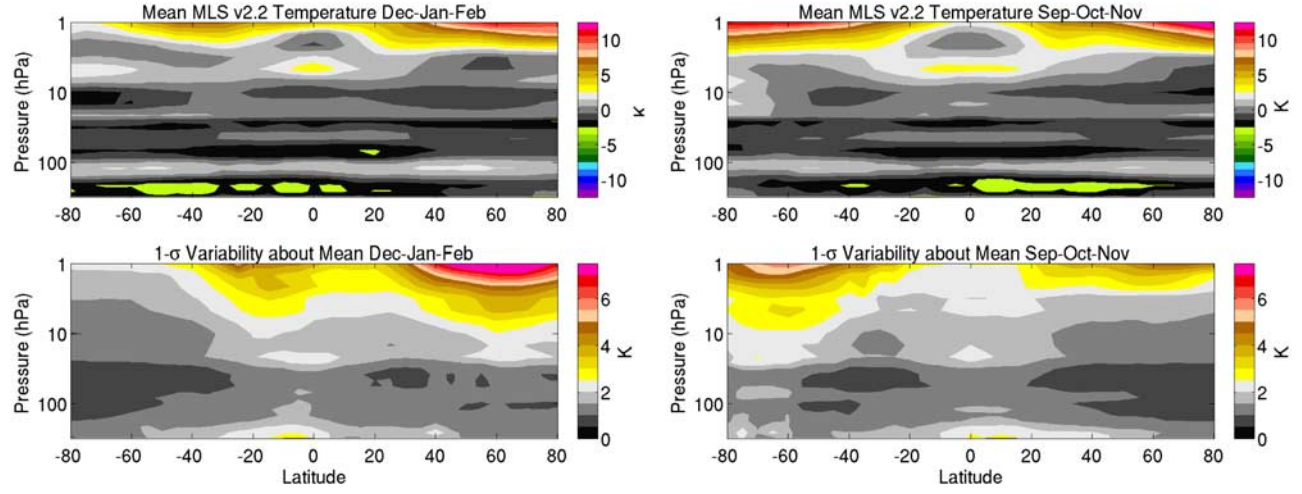


**Figure 15.** MLS minus GEOS-5 zonal mean temperature and variability averaged for December–February. A similar pattern, with north/south reversed, is seen in southern winter.

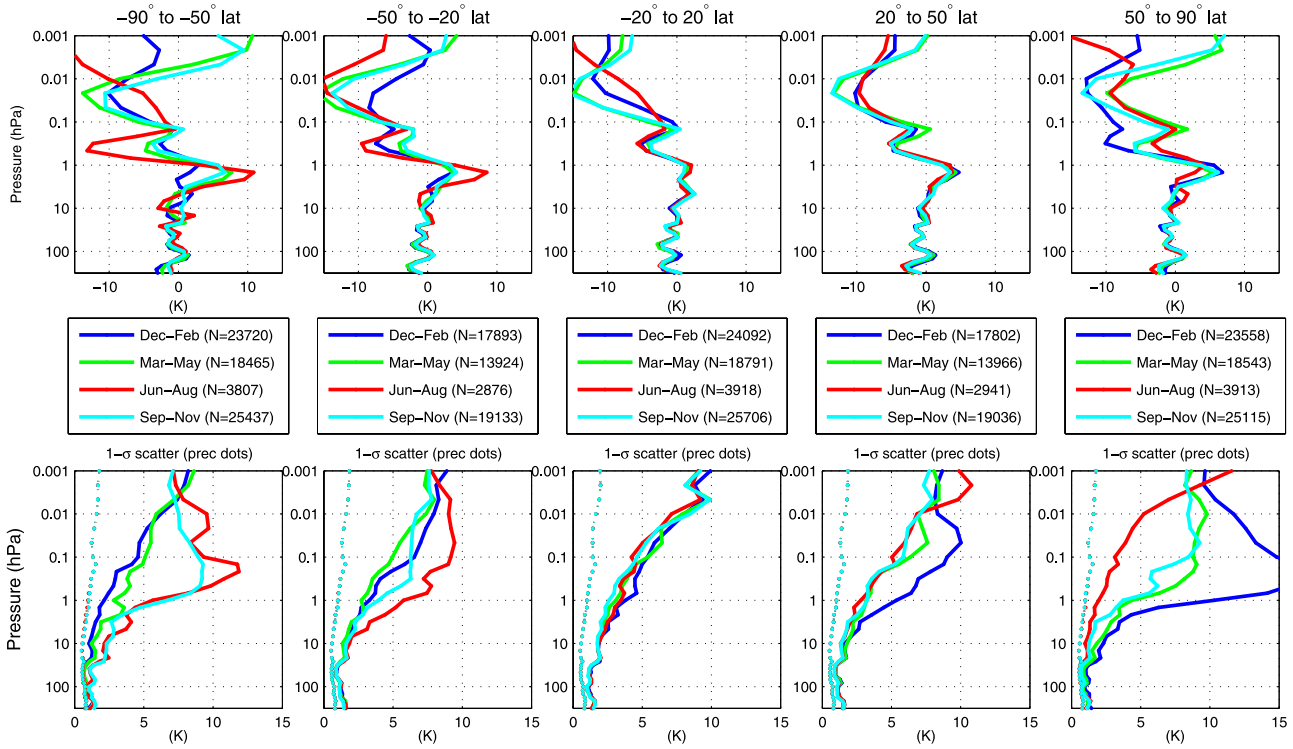


**Figure 16.** MLS v2.2 temperature minus its a priori. On this figure, and on several to follow, the top plots are zonal mean differences with colored lines indicating seasons. The bottom plots show the 1-$\sigma$ scatter (standard deviation) about the mean. Dotted lines on the bottom plots are estimated precision from the MLS retrieval. The values, N, on the legends indicate the number of profiles that were averaged in each bin. Data are from 93 days selected for initial v2.2 processing from September 2004 to January 2007.

degraded to the MLS retrieval grid by finding the log-pressure-linear interpolation between MLS grid points that best fits ECMWF, in a least squares sense. Profiles have not been convolved with MLS averaging kernels. The vertical structure of the temperature biases, shown in the top plots of Figure 17, has less than 1 K variability between seasonal and latitudinal bins from 316 hPa to 10 hPa. At these levels, the scatter between MLS and ECMWF (shown in Figure 17, bottom) is ∼1 K, which approaches MLS single measurement precision. In the upper stratosphere and mesosphere, the agreement between MLS and interpolated ECMWF becomes poorer and both biases and scatter have more seasonal and latitudinal variability. MLS has a low bias of −5 K to −12 K at 0.316 hPa. Winter high northern latitudes have scatter of 5–12 K between 1 hPa and 0.1 hPa.

### 3.3. CHAMP GPS Occultation

[57] The CHAllenging Minisatellite Payload (CHAMP) [*Wickert et al.*, 2001; *Hajj et al.*, 2004], launched into low-Earth orbit in 2000, uses GPS radio occultation to obtain profiles of temperature. Phase delays in GPS signals are measured as the line-of-sight between a GPS satellite and the CHAMP satellite passes through the atmospheric limb and is bent by refractive-index gradients. Clock precisions do not contribute significantly to measurement error, and measurement accuracy does not drift appreciably over time. Intercomparison of temperature profiles from CHAMP and the similar SAC-C satellite are consistent to 0.05–0.1 K in mean and 0.5 K in standard deviation [*Hajj et al.*, 2004].

[58] This study uses CHAMP profiles processed at the Jet Propulsion Laboratory using v2.3 and v2.4 algorithms, publicly available through http://genesis.jpl.nasa.gov. These data versions are initialized with ECMWF temperature at 40 km, and the retrieval solves for temperature from the top down. The accuracy of the measurement technique is discussed by *Kursinski et al.* [1997]. Above 30 km, the a priori may significantly influence profiles, but below 25 km, a priori influence is less than 0.2 K. Below the 250 K level in the tropospheres, the ambiguity between water and dry-air refractivity becomes significant, and temperature accuracy is degraded. GPH accuracy is better than 40 m between 5 km and 30 km.

[59] CHAMP temperature between 10 and 35 km height has a mean bias of less than 0.4 K with respect to ECMWF analyses and with respect to radiosonde data, and these differences have a height-dependent standard deviation of ∼1 K at 10 km and ∼2 K at 30 km [*Wickert et al.*, 2004].

[60] 1525 CHAMP-MLS profile pairs, coincident within 250 km and 3 hours, were identified in the first 94 days to be processed with MLS v2.2 algorithms. Figure 18 shows global averages of MLS minus CHAMP, as well as MLS minus GEOS-5 and MLS minus ECMWF at the CHAMP coincidence points. In Figure 18, CHAMP has been fit to the MLS levels with the same least squares method used in section 3.2, also not been convolved with the MLS averaging kernels. Convolution with averaging kernels does not reduce mean biases. The mean biases between MLS and the

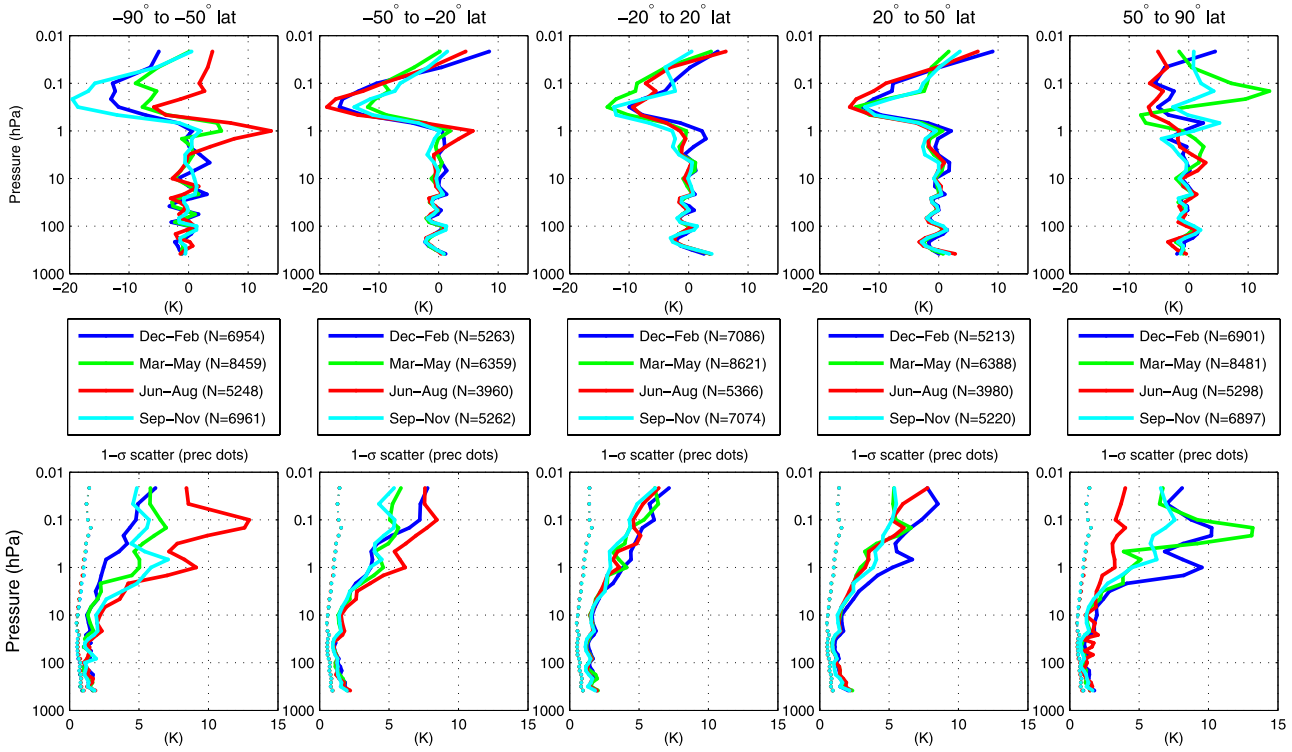


**Figure 17.** MLS v2.2 temperature minus interpolated ECMWF temperature are shown binned by latitude and season as in Figure 16. The dashed lines on the bottom plots are typical MLS individual-profile precisions. Biases from 316 hPa to 1 hPa are similar for all latitudes and seasons. Individual-profile scatter about the mean biases in seasonal/latitudinal bins is ∼1.5 K or less from 316 hPa to 10 hPa. These ECMWF data are from T799/91 only.

other three data sets, shown in Figure 18 (left), agree to better than 1 K at most MLS retrieval levels between 316 hPa and 10 hPa. GEOS-5 and ECMWF are assimilating some of the same observations, but CHAMP is an independent observation of temperature. The common bias observed here is therefore likely to be a bias in the MLS measurement. Figure 18 (right) shows the 1-$\sigma$ scatter between the comparison pairs. The MLS-GEOS-5 and MLS-ECMWF standard deviations are very similar, with the MLS-ECMWF line 0.2–0.3 K higher. MLS-CHAMP scatter is larger than that with GEOS-5 by ∼1 K from 14.7 hPa to 215 hPa. That scatter with the correlative data set (CHAMP) is not smaller than scatter with a priori is somewhat disappointing, but reflects both that CHAMP resolves vertical structure that MLS cannot, and the high degree to which GEOS-5 is a good representation of the atmosphere at these levels.

[61] Figure 19 bins the MLS-minus-CHAMP by latitude and season, with mean MLS-minus-CHAMP differences (Figure 19, top) and standard deviation of the differences about the means (Figure 19, bottom). Scatter in the summer high latitudes is ∼1 K between 100 hPa and 31.6 hPa, increasing to 2 K at 10 hPa and increasing to ∼2.5 K at 316 hPa. In the tropics, the scatter is 1.5–2 K from 316 hPa to 14.7 hPa, increasing above to 4 K at 3.16 hPa, where the accuracy of CHAMP retrievals is degraded by residual ionospheric noise and increasing sensitivity to a priori information.

[62] Figure 20 shows scatterplots of selected levels. CHAMP minus GEOS-5 is on the x axis and MLS minus GEOS-5 is on the y axis. Poor correlations indicate that MLS is generally not capturing much information in CHAMP that is not also in GEOS-5.

### 3.4. AIRS/AMSU

[63] The Aqua satellite, which is in the same orbit as Aura, approximately 15 minutes ahead, carries three nadir-sounding instruments that have been used to produce a combined temperature product: the Atmospheric Infrared Sounder (AIRS) is a thermal-infrared grating spectrometer with 2378 spectral channels between 0.4 $\mu$m and 15.4 $\mu$m [*Pagano et al.*, 2003]; the Advanced Microwave Sounding Unit (AMSU) is a nadir microwave radiometer with 15 channels between 50 GHz and 90 GHz; a second microwave instrument, the Humidity Sounder for Brazil (HSB) failed prior to Aura launch [*Lambrigtsen*, 2003] in February 2003.

[64] The AIRS/AMSU/HSB version 4 temperature product [*Chahine et al.*, 2006; *Susskind et al.*, 2003, 2006] has a nadir footprint approximately 50 km in diameter, commensurate with the AMSU field of view. The AIRS/AMSU temperature profiles shown by *Divakarla et al.* [2006] and *Tobin et al.* [2006] agree with collocated radiosondes to within about 1 K in the troposphere and lower stratosphere. *Gettelman et al.* [2004] show similar agreement in the upper troposphere using aircraft observations. *Susskind et al.* [2006] show agreement to about 1 K up to the lower stratosphere in comparisons with European Center for Medium-range Weather Forecast (ECMWF) reanalyses.

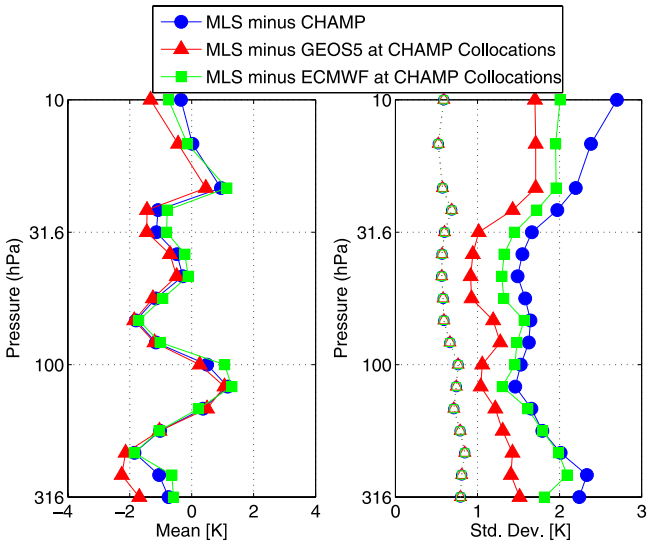


**Figure 18.** MLS v2.2 temperature minus CHAMP temperature, global average of 1525 profile pairs within 250 km and 3 hours of one another. Open symbols on the right-hand plot are average MLS single-profile precision.

The ECMWF temperatures are strongly influenced by both operational radiosondes and operational AMSU instruments. The AIRS-ECMWF differences in *Susskind et al.* [2006] increase to 2.5 K at around 2 hPa. *Susskind et al.* [2003] demonstrate, through simulation, that AIRS vertical resolution is approximately 1 km. However, AIRS vertical resolution has not been established with AIRS retrieved profiles. The AIRS/AMSU observations include products compared with MLS retrievals in other studies. *Kahn et al.* [2007] examined cloud quantities, and *Read et al.* [2007] and E. J. Fetzer et al. (Comparison of upper tropospheric water vapor observations from the Microwave Limb Sounder and Atmospheric Infrared Sounder, submitted to *Journal of Geophysical Research*, 2008) compare water vapor from the two instruments.

[65] The MLS limb track is well-collocated with the center of the AIRS swath. Since MLS views forward along the orbital track at the atmospheric limb, MLS limb tangent points are only 7–8 minutes behind the AIRS nadir observations. In this study six AIRS/AMSU profiles, three on each side of nadir and closest in latitude to a given MLS profile, are averaged to give a profile collocated with MLS. AIRS temperature data are screened to remove the impact of clouds, as described by *Aumann et al.* [2005] and *Susskind et al.* [2006]. The resulting cloud-cleared, 150-km-along-track average by 100-km-across-track average AIRS temperature includes an MLS limb path that will come 8 minutes later.

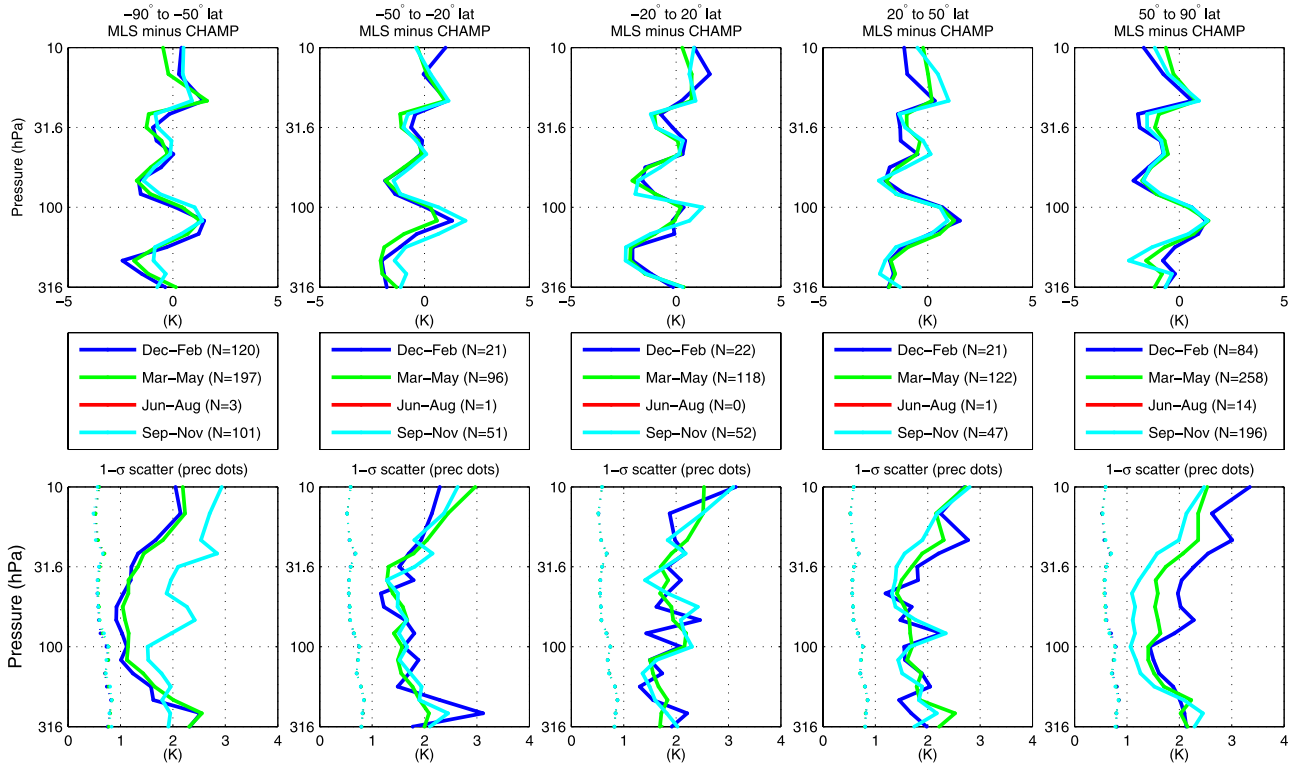


**Figure 19.** MLS v2.2 temperature minus CHAMP temperature, averaged in latitudinal and seasonal bins, as in Figure 16. The number of MLS profiles averaged, for each bin, is shown (N) in the middle row. Solid lines in the bottom row are the 1-$\sigma$ standard deviation of profiles about the mean profile of a given bin. Dotted lines are the average combined estimated precisions of a single MLS profile. The June–August lines have been removed because not enough coincidences have been found to give useful statistics.

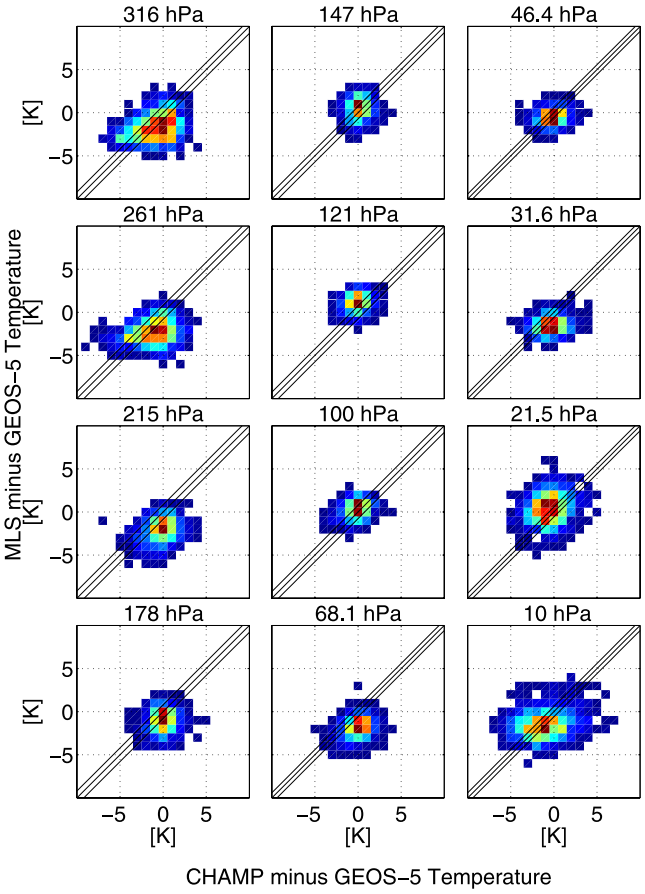


**Figure 20.** Scatter of MLS-minus-GEOS-5 and CHAMP-minus-GEOS-5 are shown. Colors are normalized to peak of distribution, with "hotter" colors indicating higher probability. The outer black lines are at plus and minus the MLS estimated precision (based upon radiance noise propagated through the measurement system) from the 1:1 line.

[66] MLS has biases with respect to AIRS/AMSU in the upper troposphere and lower stratosphere that are very similar to those that have been seen with respect to other correlative data sets, as can be seen in the summary provided by Figure 26. Figure 21 bins biases and scatter by latitude and season. The oscillatory behavior between 10 hPa and 1 hPa for March–May and June–August in the 90°S–50°S latitude bin is also seen in SABER comparisons of section 3.5, and warrants further investigation. At 0.1 hPa, AIRS/AMSU is ~10 K warmer than MLS in most latitudinal-seasonal bins, and 5–10 K warmer than ACE, SABER and HALOE.

### 3.5. SABER

[67] The Sounding of the Atmosphere using Broadband Radiometry (SABER) [*Mlynczak and Russell*, 1995] instrument, launched on the Thermosphere Ionosphere Mesosphere Energetics and Dynamics (TIMED) satellite in December, 2001, measures profiles of kinetic temperature using 15-$\mu$m and 4.3-$\mu$m $CO_2$ limb-emission radiance measurements. Pressure is measured from spectral contrast between channels, and temperature is then inferred from pressure and pointing heights assuming hydrostatic equilibrium. The effective vertical resolution of the SABER temperature profiles is ~2 km although it is retrieved on a higher-resolution fixed set of pressure surfaces [*Remsberg et al.*, 2003]. Version 1.06 SABER temperature, used in this study, has been extensively validated [*Remsberg et al.*, 2002, 2003].

[68] The 24,577 pairs of MLS and SABER profiles within 2 degrees of great circle arc (220 km) and 3 hours in time are compared. SABER retrieved values are provided at tangent points that sweep through a range of latitudes and longitudes, covering on the order of 300 km in a single profile, but for this study, the SABER profile location is taken from ~0.1 hPa, near the midpoint of the profile. Collocations at the extreme ends of the profile are generally better than 370 km. SABER data have been interpolated to MLS observation points using the least squares method discussed in section 3.2. Differences between interpolated SABER and the MLS a priori temperatures are convolved with the MLS averaging kernels to degrade SABER to MLS's vertical resolution, which is significantly poorer than its measurement grid in the upper mesosphere and lower thermosphere.

[69] Non-local-thermodynamic equilibrium (non-LTE) effects in the very cold conditions (~130 K) of the summer polar mesopause (temperature minimum near 85 km) are not modeled in SABER v1.06, leading to a mesopause which is 3–5 km too low compared to falling spheres experiments, lidar observations and climatology [*Kutepov et al.*, 2006]. Version 1.07 of the SABER data corrects for non-LTE, lowering in altitude and warming the mesopause, but was not available at the time of this study. Non-LTE effects are not significant when temperature is above ~170 K (M. Mlynczak, personal communication, 2007).

[70] Figure 22 shows global comparisons of coincident SABER and MLS profiles. MLS has a cold bias with respect to SABER at 100–10 hPa of 2 to 3 K with an additional oscillation of ~2 K peak-to-peak, similar to that seen in other correlative data sets. The bias of −4 to −5 K at 261 hPa is larger in magnitude than is seen in comparisons with other data sets. Through most of the decade 10–1 hPa MLS has a −1 K bias compared to SABER, however at 1 hPa, MLS has a 3 to 5 K high bias, and at 0.46–0.38 hPa a −3 to −5 K low bias.

[71] In the summer polar mesosphere (red line on the 50°N–90°N plot and blue line on the 50°S–90°S plot) MLS has a large positive bias at 0.01 hPa (+12 K north, +7 K south) and a low bias at 0.001 hPa which is generally consistent with the anomalously low mesopause in v1.06 SABER data.

[72] The 1-$\sigma$ scatter (standard deviation) of MLS minus SABER from 100–10 hPa is ~1 K in many of the latitude/seasonal bins, and is less than 1 K in the summer high latitudes. This scatter results from the combined precision and accuracy of the MLS and SABER measurements as well as atmospheric variability sampled with imperfect coincidences; it may be taken as an upper bound on MLS precision at these levels. The larger variability observed in the winter poles results from differences between MLS and SABER sampling and the large temperature gradients associated with the winter polar vortices. In the decade 10–1 hPa the summer polar bins' scatter increases from 1–2.5 K and from 1–0.1 hPa increases from 2.5 K to 3 K. Other

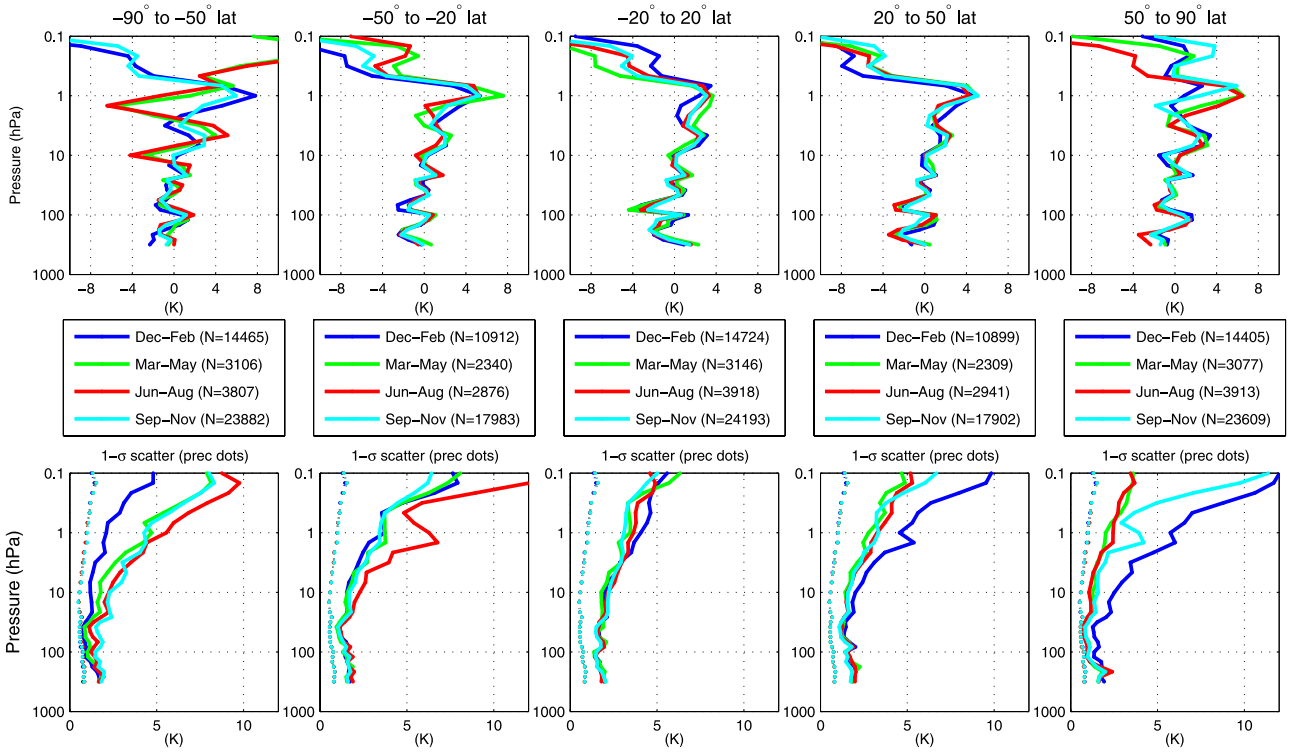


**Figure 21.** MLS v2.2 temperature minus AIRS/AMSU v4.0.9 temperature, averaged in latitudinal and seasonal bins, as in Figure 16. The number of MLS profiles averaged, for each bin, is shown (N) in the middle row. Solid lines in the bottom row are the 1-$\sigma$ standard deviation of profiles about the mean profile of a given bin. Dotted lines are the average combined estimated precisions of a single MLS profile and the AIRS/AMSU profiles to which it was compared.

latitude/seasonal bins have scatter of 3–5 K in the 1–0.1 hPa decade except for southern summer bins, which are 5–7 K. From 0.1–0.001 hPa, scatter increases from ~5 K to 12–15 K in all bins.

[73] Figure 23 (six left plots) scatter global SABER temperature versus MLS temperature at six representative levels. The cluster of outlier points at 0.01 hPa near 150 K with a low SABER bias relative to MLS and those at 0.001 hPa with MLS temperatures 120–140 K and a high SABER bias relative to MLS are qualitatively consistent with the effects of non-LTE on SABER v1.06 at the very low temperatures of the summer polar mesosphere. Figure 23 (six right plots) show the scatter of SABER minus MLS a priori with MLS minus MLS a priori. Points where SABER temperature is less than 170 K have been removed. Global averages of the biases shown on Figure 22 for these six levels are evident as a 2 K low bias of MLS at 10 hPa, a 3–4 K high bias of MLS at 1 hPa and a 5–10 K low bias of MLS at 0.001 hPa. At 10 hPa there is some positive correlation, and at lower pressures, where CIRA climatology is the a priori, higher levels of correlation are evident. The elongated distribution of SABER scatter relative to a priori at 100 hPa comes primarily from the December–February northern high latitudes and the September–November bin of the southern high latitudes, as seen in Figure 22. Figure 24 shows zonal mean curtain plots for November 12, 2004, a day on which MLS and SABER had local solar time coincidences of better than 1.5 hours from 20° S to 70° N latitudes, limiting the impact of tides on coincident-profile pairs. Agreement between MLS and SABER is quite good into the lower mesosphere.

[74] MLS resolves something of the layered mesopause structure seen in SABER near 0.01 hPa, 30° S to the equator, but nothing of the vertical structure at 0.001 hPa at the equator. Above the 0.1 hPa surface, MLS is on 3 levels-per-decade and its vertical resolution is 10 km or poorer. At these levels, SABER data, which have not been degraded to MLS resolution, have 1.5x–2x more zonal variability than does MLS. MLS data are shown at pressures below 0.001 hPa, but these levels are not recommended for scientific use.

### 3.6. HALOE

[75] The Halogen Occultation Experiment (HALOE) on UARS measured profiles of limb path solar attenuation in eight infrared bands. These measurements are used to infer profiles of temperature, as well as gas mixing ratios of seven species and aerosol extinction. The HALOE temperature retrieval has been extensively validated [*Hervig et al.*, 1996; *Remsberg et al.*, 2002].

[76] The HALOE V19 temperature is used in this study from 35 km to ~85 km, where the signal-to-noise ratio decreases to unity. At heights below 35 km altitude, aerosol significantly impacts HALOE measurements, and the HALOE V19 files report NCEP temperature. Between 35 km and 45 km, HALOE V19 makes a linear transition from NCEP temperature to temperature derived from occultation data. The typical measurement uncertainty,

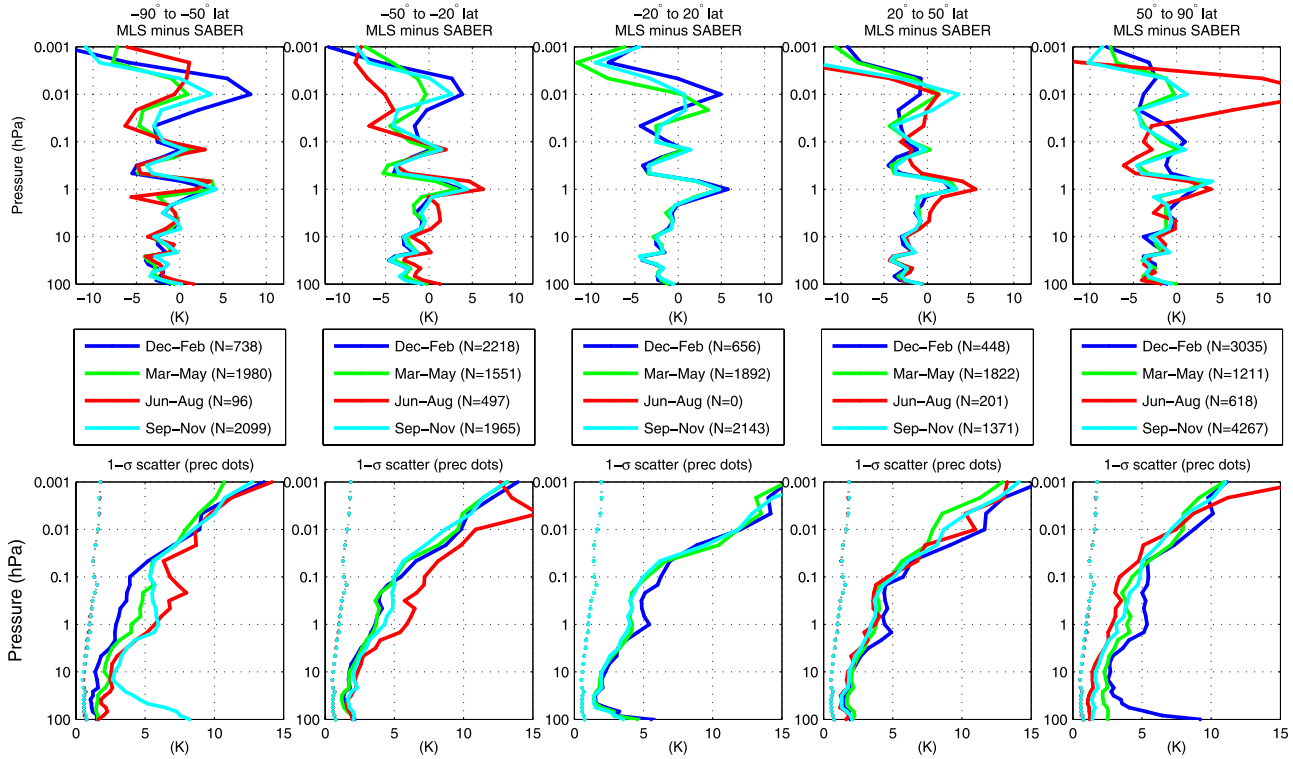


**Figure 22.** MLS v2.2 temperature minus SABER temperature, averaged in latitudinal and seasonal bins, as in Figure 16. The number of MLS profiles averaged, for each bin, is shown (N) in the middle row. Solid lines in the bottom row are the 1-$\sigma$ standard deviation of profiles about the mean profile of a given bin. Dotted lines are single-profile estimated precisions based upon propagated MLS radiometric noise.

including random and systematic errors, is 5 K below 80 km [*Hervig et al.*, 1996; *Remsberg et al.*, 2002].

[77] An improved HALOE product correcting for the effect of Polar Mesospheric Clouds (PMCs) was not available for this study. PMCs can cause high biases in V19 temperature of up to 10 K [*McHugh et al.*, 2003].

[78] Four-hundred-forty-one coincident HALOE profiles were found within 500 km and 6 hours of an MLS profile from September 2004 through November 2005. Several days with good latitudinal coverage in the MLS-HALOE coincidences were reprocessed with MLS v2.2. No profile pairs are closer than 3 hours, and the mean absolute value of time difference is 4.4 hours.

[79] Differences between collocated MLS and HALOE profiles are shown in Figure 25. The number of profiles is not sufficient to show latitudinal and seasonal variation. The coincidences shown are the closest MLS profile to a HALOE profile within 500 km and 6 hours. As a result of the 160 km along-track sampling of MLS, the "best" matched MLS profile is only very rarely more than 150 km away from its HALOE match in the meridional direction. HALOE has a less sharp stratopause than MLS, with a ~2 K warm bias with respect to MLS near 2.15 hPa, a 1 K cold bias at 1 hPa and a mesosphere which is generally warmer (by as much as 6 K at 0.316 hPa.)

### 3.7. ACE-FTS

[80] The Atmospheric Chemistry Experiment (ACE) was launched on the Canadian SCISAT-1 satellite on 12 August 2003 [*Bernath et al.*, 2004]. Its primary instrument is the ACE Fourier Transform Spectrometer (ACE-FTS), which will be referred to simply as ACE in this work, views sunrise and sunset occultations by the atmospheric limb with an infrared (2.2–13.3 $\mu$m) Fourier transform spectrometer that has 0.02 $cm^{-1}$ spectral resolution. It is in a 74° inclination orbit that accumulates measurements of global coverage over one year, with extended periods viewing only at high latitudes. It has a vertical resolution of ~4 km. The ACE temperature retrieval process is described in detail by *Boone et al.* [2005]. Briefly, 106 spectral lines of CO2 between 930 and 3380 $cm^{-1}$ are analyzed to determine pressure and temperature from the troposphere to the lower thermosphere. The current version of the ACE retrieval is 2.2. Initial validation studies using ACE version 1.0 have shown agreement between ACE and HALOE of ±2 K [*McHugh et al.*, 2005], of better than ±2.5 K with radiosondes from 10–30 km [*Kerzenmacher et al.*, 2005], and of better than ±2.5 K with lidar measurements from 17–45 km [*Kerzenmacher et al.*, 2005].

[81] Eight-hundred-ninety-four MLS-ACE coincident profile pairs were identified in the first 93 days processed with MLS v2.2 algorithms. Coincidences were within 6 hours and within 10 degrees of longitude. MLS 1.5-degree along track sampling guarantees that the best coincident profiles match within 1 degree of latitude. Figure 26 (yellow triangles) shows global mean biases (left) and standard deviations of differences (right) between MLS and ACE profiles. ACE and SABER are 1–2 K warmer than other

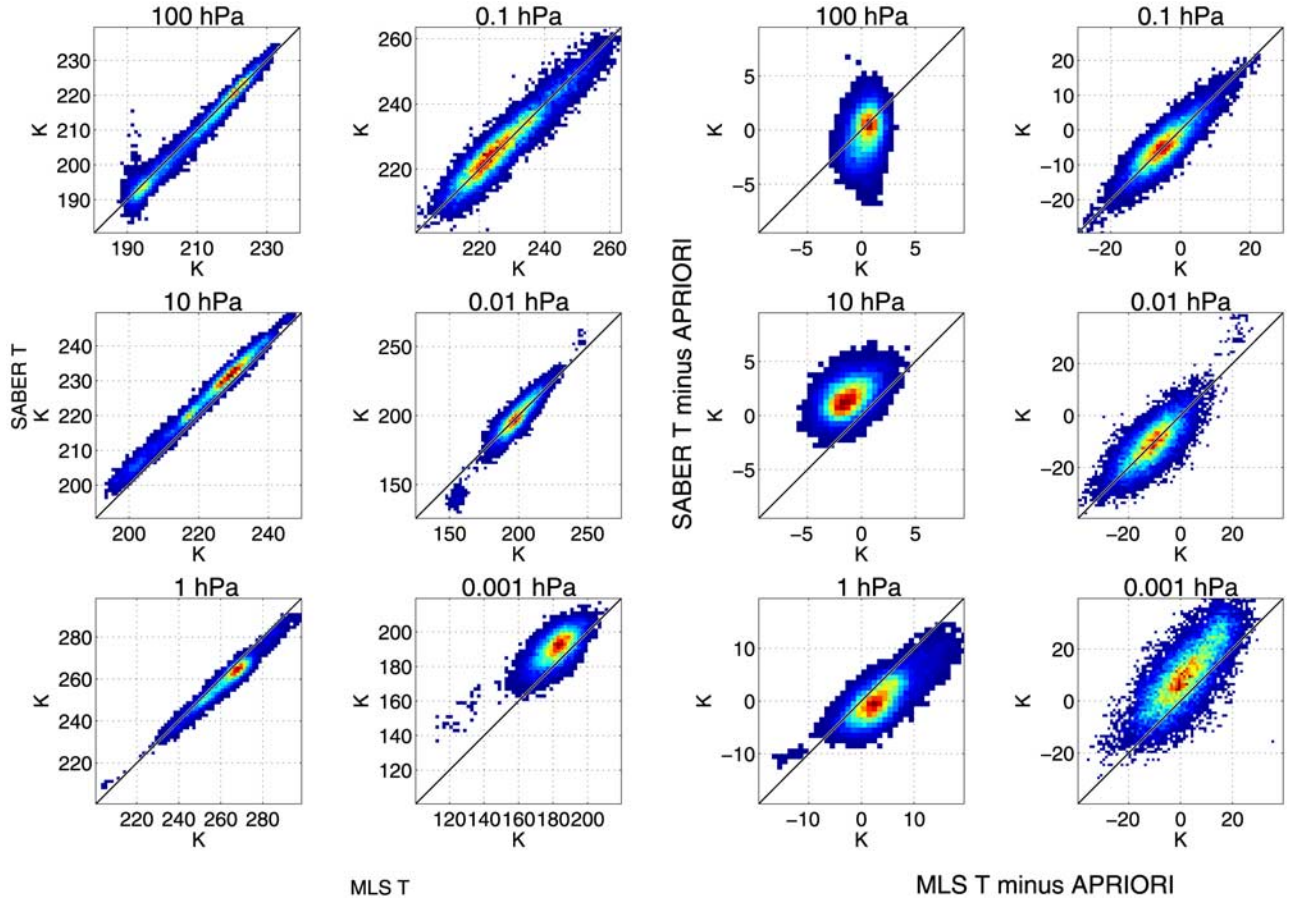


**Figure 23.** Six left plots are SABER temperature scattered against MLS temperature for six representative levels. Six right plots are SABER minus MLS a priori versus MLS minus MLS a priori for the same levels. Points with SABER temperature less than 170 K have been excluded from the right-hand side.

correlative data sets in the stratosphere. ACE is 5–7 K warmer than MLS from 0.1 hPa to 0.02 hPa, and 10 K warmer than MLS at 0.001 hPa.

### 3.8. Temperature Comparison Summary

[82] The global mean bias of MLS temperature relative to eight correlative data sets is shown in Figure 26. Between 316 hPa and 10 hPa, MLS has global biases with respect to ECMWF, GEOS-5, AIRS, radiosondes and CHAMP that agree to within ∼1 K. SABER, ACE and HALOE (which has valid data starting at 4.6 hPa) are generally warmer by 1–3 K in the stratosphere, but have similar vertical structure in their global biases with respect to MLS. Estimates of MLS systematic uncertainties are also shown. The black line is the predicted effect of amplifier gain compression based upon laboratory measurements of MLS flight-hardware-spare intermediate amplifiers, and the gray shading about the black line is the 2-$\sigma$ envelope of the combined systematic uncertainties discussed in section 2.6. The gain-compression model explains most of the vertical structure of observed biases in the upper troposphere and stratosphere, although it predicts an unobserved ∼4-K bias at 21.5 hPa. In the mesosphere, the gain-compression model predicts that MLS would have a warm bias of 0–3 K, and other sources of systematic uncertainty are not large enough to explain the generally 0–7 K cold bias of MLS relative to SABER, ACE and HALOE.

### 3.9. GPH Comparisons

[83] MLS v2.2 100 hPa GPH is typically 100–250 m higher than GEOS-5 in the northern high latitudes and 50–200 m higher than GEOS-5 in the Southern high latitudes. At low latitudes, the ascending branch of the orbit is typically 0–120 m higher than GEOS-5 while the descending branch is 100–200 m higher. A seasonal cycle in the daily mean differences of ∼100 m peak-to-peak is evident in the high-southern latitudes (peaking in January) and in the ascending branch of the equatorial mean differences (peaking in July) There has been a general downward trend in the MLS minus GEOS-5 bias of 40–50 m/year over the life of the mission. Correction of gain compression, which is neglected in v2.2 retrievals, lowers MLS 100 hPa GPH by ∼150 m, bringing it into better agreement with GEOS-5. The gain-compression parameter has not been tuned to match observed temperature or GPH biases, but rather was measured in the laboratory using spare flight hardware. MLS v2.2 GPH has a bias of ∼100 m at 10 hPa with respect to GEOS-5 and SABER, and the bias with respect to SABER becomes increasingly negative at lower pressures: ∼−100 m at 0.01 hPa and ∼−500 m at 0.001 hPa. These negative biases reflect the general low temperature bias of MLS with respect to SABER.

[84] Figure 27 shows globally averaged differences between MLS GPH and SABER GPH and between MLS

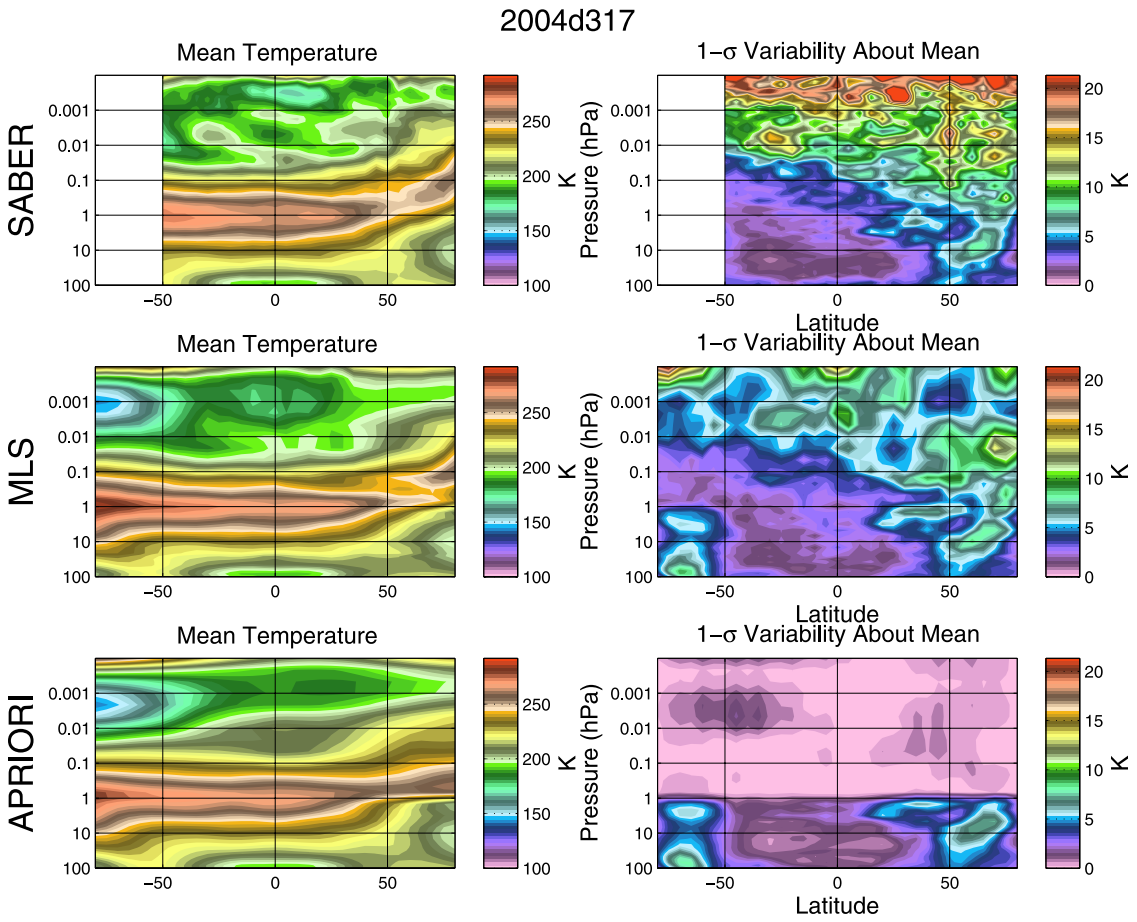


**Figure 24.** SABER descending, MLS ascending and MLS a priori temperature zonal means for 12 November 2004. MLS ascending and SABER descending branches are within 1.5 hours of local solar time from 20°S–70°N on this day. MLS a priori temperature is GEOS-5 at levels below 1 hPa and CIRA86 climatology above. SABER data on this plot have been interpolated to 12 levels-per-decade of pressure and have not been convolved with MLS averaging kernels. The color spacing on the left-hand, zonal-mean plots is 3 K.

GPH and GEOS-5 GPH. The slopes of the curves on the left-hand plot are proportional to the average temperature difference between the two data sets at a given level. In both cases, the increasingly large low bias of MLS GPH with height results from an overall low bias in MLS temperature relative to the correlative data sets. GEOS-5 is expected to be the more reliable of these two correlative data sets in the troposphere and lower stratosphere, where it is well-supported by assimilated sondes and other measurements. In the mesosphere, SABER has good sensitivity and should be preferred to GEOS-5. In the upper stratosphere, there is generally good agreement between the two correlative data sets. The ability of the MLS GPH to accurately represent wave motions from the upper troposphere through the mesosphere makes it a useful product for dynamical studies of the middle atmosphere.

## 4. Conclusions and Future Plans

[85] Version 2.2 of the MLS data processing algorithms produces temperature profiles that are considered scientifically useful at pressures from 316 hPa to 0.001 hPa. In the upper troposphere and lower stratosphere, comparisons of

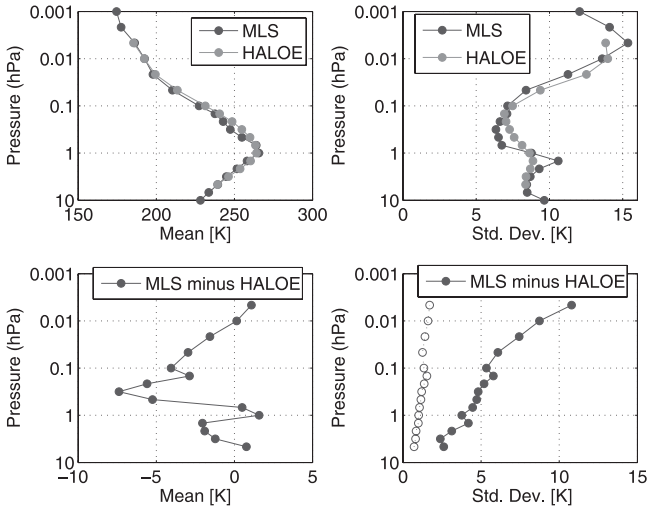


**Figure 25.** Globally averaged MLS v2.2 temperature minus HALOE V19 temperature. (top) The means and standard deviations of collocated MLS and HALOE profiles. (bottom) The mean and standard deviation of the difference.

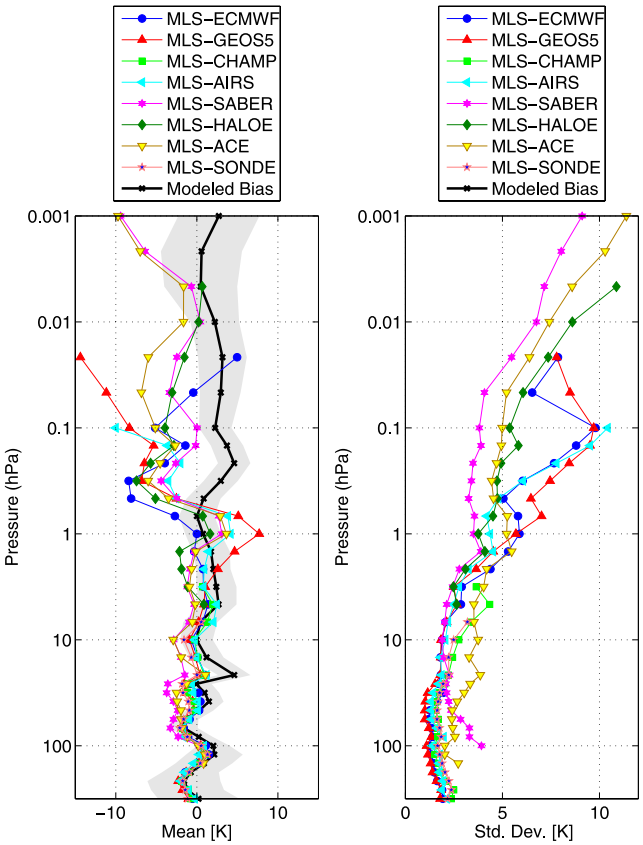


**Figure 26.** Summary of temperature biases and scatter between MLS and eight correlative data sets. (left) Mean differences and (right) scatter about these differences. Modeled systematic uncertainties (discussed in section 2.6) are also shown, with gain compression in black and the 2-$\sigma$ contribution of the other terms, which are biases of unknown sign, summarized by the gray envelope. Mean differences from 3.16 hPa to 0.1 hPa are correlated among the comparisons and likely indicate a bias in MLS measurements.

v2.2 temperature with correlative data sets show that MLS has persistent systematic biases with a ~3-K peak-to-peak vertical structure. Most of this vertically varying bias is reproduced by a model of MLS amplifier gain compression. The model was in no way tuned to match observed temperature biases but, rather, had its parameters set by laboratory measurements of spare flight hardware.

[86] The global mean bias relative to eight correlative data sets can be seen in Figure 26. Between 316 hPa and 10 hPa, most correlative data sets agree with one another within ~1 K, and most of the common systematic bias is explained by gain compression (nonlinearity) in MLS spectrometer amplifiers, which was neglected in the v2.2 instrument forward model.

[87] Table 1 summarizes precision, resolution, observed scatter and modeled and observed biases for temperature and GPH. Table 1, third column, lists retrieval precision that is based upon the propagation of radiance measurement uncertainty through the retrieval software. These precisions range from 0.6 K in the lower stratosphere to 2.5 K in the mesosphere and to 1 K at 316 hPa. Table 1, fourth column, contains an estimate of temperature precision based upon differences between pairs of observations, separated by one orbit, at latitudes and seasons where longitudinal variability is small. The vertical and horizontal resolution of the temperature and GPH products is shown in the second column of Table 1. The across-track beam width is 6–12 km.

[88] The accuracy of MLS temperature and GPH has been estimated both by propagating uncertainty in measurement and retrieval parameters through the measurement system (Table 1, fifth column, for temperature and eighth column for GPH), and using observed biases relative to correlative data sets (Table 1, sixth column for temperature and ninth column for GPH.) The modeled uncertainty estimates are broken into two pieces; the first term is due to amplifier "gain compression" and has a known sign while the second term includes effects of spectroscopic parameters, retrieval numerics and pointing for which the sign of resulting bias is unknown. Gain compression results in a global temperature bias profile of −1.5 K to +4.5 K, with significant vertical structure. Simulations suggest that this bias does not have significant latitudinal dependence. Systematic temperature uncertainties of unknown sign are of ~2 K magnitude over most of the retrieval range, increasing to 5 k at 316 hPa and to 3 K at 0.001 hPa.

[89] Table 1 sixth column, contains estimates of temperature accuracy based upon observed biases between MLS and collocated correlative profiles. In the troposphere and lower stratosphere, the estimated biases are consistent to within ~1.5 K between most of the correlative data sets, as may be seen in Figure 26. A persistent vertical oscillation must be presumed to be in the MLS measurement. This oscillation has an amplitude of 2–3 K and a frequency of about 1.5 cycles per decade of pressure. From 316 hPa to ~10 hPa there is generally agreement to ~1 K between the assimilations (ECMWF and GEOS-5) and AIRS, radiosondes and CHAMP, which show consistent biases with respect to MLS. SABER and ACE have generally warm biases of ~2 K relative to this group.

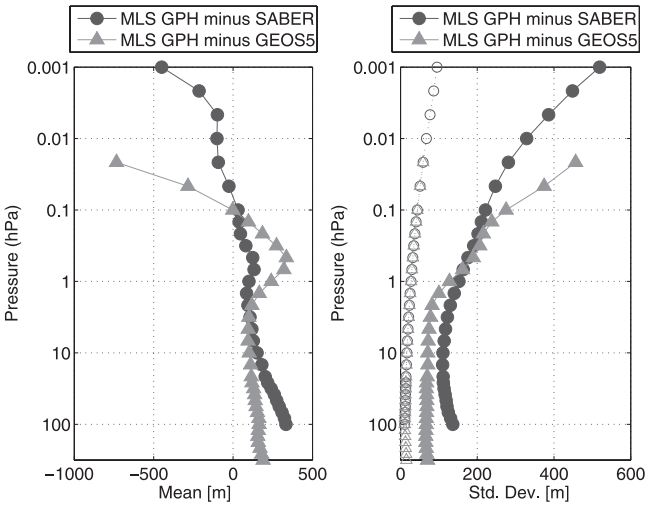


**Figure 27.** Globally averaged MLS GPH minus SABER GPH (gray) and MLS GPH minus GEOS-5 GPH (black) averaged over the same profile pairs.

**Table 1.** Summary of MLS Temperature and GPH Products

| Pressure, hPa | Resolution Vertical × Horizontal, km | Temperature Precision,[a] K | Temperature Scatter, [b] K | Modeled Temperature Bias Uncertainty, K | Observed Temperature Bias, K | GPH Precision,[a] m | Modeled GPH Bias Uncertainty, m | Observed GPH Bias, m |
|---|---|---|---|---|---|---|---|---|
| <0.001 | NR[c] | | | | | | | |
| 0.001 | 15 × 220 | ±2.5 | ±3.5 | +2 ± 3 | −9 | ±110 | +700 ± 150 | −450 |
| 0.01 | 14 × 185 | ±2.2 | ±3 | +2 ± 3 | −2... 0 | ±85 | +600 ± 100 | −100 |
| 0.1 | 9.1 × 170 | ±2 | ±2.3 | +2 ± 2 | −8... 0 | ±60 | +500 ± 150 | 0 |
| 0.316 | 8.3 × 165 | ±1 | ±1.5 | +3 ± 2 | −7... −4 | ±50 | +400 ± 120 | 50 |
| 1 | 7.9 × 165 | ±1 | ±1.4 | +1 ± 2 | 0... +5 | ±45 | +300 ± 100 | 100 |
| 3.16 | 6.2 × 165 | ±0.8 | ±1 | +2 ± 2 | +1 | ±40 | +250 ± 100 | 100 |
| 10 | 4.3 × 165 | ±0.6 | ±1 | 0 ± 2 | −1... 0 | ±35 | +200 ± 100 | 100 |
| 14.7 | 3.9 × 165 | ±0.6 | ±1 | −4 ± 2 | 0... +1 | ±35 | +180 ± 100 | 125 |
| 31.6 | 3.5 × 165 | ±0.6 | ±1 | +1 ± 2 | −2... 0 | ±35 | +170 ± 100 | 140 |
| 56.2 | 3.8 × 165 | ±0.8 | ±0.8 | −1 ± 2 | −2... 0 | ±35 | +160 ± 100 | 150 |
| 100 | 5.2 × 165 | ±0.8 | ±0.8 | +2 ± 2 | 0... +1 | ±30 | +150 ± 100 | 150 |
| 215 | 5.0 × 170 | ±1 | ±1 | −1.5 ± 4 | −2.5... −1.5 | ±35 | +125 ± 125 | 150 |
| 316 | 5.3 × 170 | ±1 | ±1 | 0 ± 5 | −2... 0 | ±35 | +100 ± 150 | 150 |
| >316 | NR | | | | | | | |

[a]Individual profiles estimated from propagation of uncertainty through the retrieval system.
[b]Precision estimated from scatter of observations of very similar scenes in successive orbits.
[c]Not recommended for scientific use.

[90] The structure and amplitude of tropospheric and lower stratospheric temperature biases predicted by the gain compression model is in excellent agreement with the observed biases shown in Figure 26. Gain compression also explains the ∼140-m global bias in 100 hPa GPH between MLS and GEOS-5. No parameter tuning was done to achieve this agreement. Correction for gain compression is a high priority for future versions of the MLS retrieval algorithms

[91] Biases between MLS and correlative measurements in the mesosphere are not well understood. Correction for gain compression will permit the internally consistent use of more radiances in the retrieval, and will improve vertical resolution of the temperature product in the upper stratosphere and mesosphere. Improved convergence of the temperature retrieval in the autumn and early winter poles and proper alignment of Status fields with profiles impacted by clouds are further goals of algorithm development.

[92] **Acknowledgments.** Funding for ACE was provided by the Canadian Space Agency and the Natural Sciences and Engineering Research Council (NSERC) of Canada. Work at the Jet Propulsion Laboratory, California Institute of Technology, was done under contract with the National Aeronautics and Space Administration. The ECMWF is thanked for providing their data. CHAMP data were processed at JPL and obtained from the http://genesis.jpl.nasa.gov web site, operated and maintained at JPL. Thanks go to Chi Ao and Byron Iijima for help with the CHAMP data. Thanks go to Chris Mertens from NASA Langley and the SABER data processing team at GATS, Inc. for providing SABER data. We wish to thank the Aura Project for their support throughout the years (before and after Aura launch), in particular M. Schoeberl, A. Douglass (also as cochair of the Aura validation working group), E. Hilsenrath, and J. Joiner. We also acknowledge the support from NASA Headquarters, P. DeCola for MLS and Aura, and M. Kurylo, J. Gleason, B. Doddridge, and H. Maring, especially in relation to the Aura validation activities and campaign planning efforts. We greatly appreciate the efforts of Bojan Bojkov and the Aura Validation Data Center (AVDC) team, whose work facilitated the MLS validation activities.

## References

Aumann, H., et al. (2005), AIRS/AMSU/HSB version 4.0 data release user guide, version 1.0 edition, report, Jet Propul. Lab., Calif. Inst. of Technol., Pasadena, Calif.

Bernath, P., et al. (2004), Atmospheric chemistry experiment (ACE): Mission overview, *Proc. SPIE Int. Soc. Opt. Eng.*, *5542*, 146–156.

Bloom, S., L. Takacs, A. da Silva, and D. Ledvina (1996), Data assimilation using incremental analysis updates, *Mon. Weather Rev.*, *124*, 1256–1271.

Bloom, S., et al. (2005), Documentation and validation of the Goddard Earth Observing System (GEOS) Data Assimilation System—Version 4, *TM-2005104606 VOL26 VER4*, 165 pp., NASA Goddard Space Flight Cent., Greenbelt, Md.

Boone, C., R. Nassar, K. Walker, Y. Rochon, S. McLeod, C. Rinsland, and P. Bernath (2005), Retrievals for the atmospheric chemistry experiment Fourier-transform spectrometer, *Appl. Opt.*, *44*, 7218–7231.

Chahine, M. T., et al. (2006), The atmospheric infrared sounder (AIRS): Improving weather forecasting and providing new data on greenhouse gases, *Bull. Am. Meteorol. Soc.*, *87*(7), 911–926.

Divakarla, M., C. Barnet, M. Goldberg, L. McMillin, E. Maddy, W. Wolf, L. Zhou, and X. Liu (2006), Validation of Atmospheric Infrared Sounder temperature and water vapor retrievals with matched radiosonde measurements and forecasts, *J. Geophys. Res.*, *111*, D09S15, doi:10.1029/2005JD006116.

Durre, I., R. Vose, and D. Wuertz (2004), Overview of the Integrated Global Radiosonde Archive, *J. Clim.*, *19*, 53–68.

Fleming, E., S. Chandra, J. Barnett, and M. Corney (1990), Zonal mean temperature, pressure, zonal wind and geopotential height as functions of latitude, *Adv. Space Res.*, *10*, 11–53.

Froidevaux, L., et al. (2006), Early validation analyses of atmospheric profiles from EOS MLS on the Aura satellite, *IEEE Trans. Geosci. Remote Sens.*, *44*, 1106–1121.

Gettelman, A., et al. (2004), Validation of Aqua satellite data in the upper troposphere and lower stratosphere with in situ aircraft instruments, *Geophys. Res. Lett.*, *31*, L22107, doi:10.1029/2004GL020730.

Hajj, G. A., C. O. Ao, B. A. Iijima, D. Kuang, E. R. Kursinski, A. J. Mannucci, T. K. Meehan, L. J. Romans, and T. P. Yunck (2004), CHAMP and SAC-C atmospheric occultation results and intercomparisons, *J. Geophys. Res.*, *109*, D06109, doi:10.1029/2003JD003909.

Hervig, M., et al. (1996), Validation of temperature measurements from the Halogen Occultation Experiment, *J. Geophys. Res.*, *101*, 10,277–10,285.

Kahn, B. H., A. Eldering, A. J. Braverman, E. J. Fetzer, J. H. Jiang, E. Fishbein, and D. L. Wu (2007), Toward the characterization of upper tropospheric clouds using Atmospheric Infrared Sounder and Microwave Limb Sounder observations, *J. Geophys. Res.*, *112*, D05202, doi:10.1029/2006JD007336.

Kerzenmacher, T., et al. (2005), Measurements of $O_3$, $NO_2$ and temperature during the 2004 Canadian Arctic ACE validation campaign, *Geophys. Res. Lett.*, *32*, L16S07, doi:10.1029/2005GL023032.

Kursinski, E., G. Hajj, J. Schofield, R. Linfield, and K. Hardy (1997), Observing Earth's atmosphere with radio occultation measurements using the Global Positioning System, *J. Geophys. Res.*, *102*, 23,429–23,465.

Kutepov, A., A. Feofilov, B. Marshall, L. Gordley, W. Pesnell, R. Goldberg, and J. Russell (2006), SABER temperature observations in the summer

polar mesosphere and lower thermosphere: Importance of accounting for the $CO_2$ $\nu_2$ quanta V-V exchange, *Geophys. Res. Lett.*, *33*, L21809, doi:10.1029/2006GL026591.

Lambrigtsen, B. (2003), Calibration of the AIRS microwave instruments, *IEEE Trans. Geosci. Remote Sens.*, *41*, 369–378.

Limpasuvan, V., D. Wu, M. Schwartz, J. Waters, Q. Wu, and T. Killeen (2005), The two-day wave in EOS MLS temperature and wind measurements during 2004–2005 winter, *Geophys. Res. Lett.*, *32*, L17809, doi:10.1029/2005GL023396.

Lin, S. (2004), A "vertically Lagrangian" finite-volume dynamical core for global models, *Mon. Weather Rev.*, *132*, 2293–2307.

Livesey, N. J., and W. G. Read (2000), Direct retrieval of line-of-sight atmospheric structure from limb sounding observations, *Geophys. Res. Lett.*, *27*, 891–894.

Livesey, N. J., W. V. Snyder, W. G. Read, and P. A. Wagner (2006), Retrieval algorithms for the EOS Microwave Limb Sounder (MLS), *IEEE Trans. Geosci. Remote Sens.*, *44*, 1144–1155.

Livesey, N. J., et al. (2007), EOS MLS version 2.2 level 2 data quality and description document, *Tech. Rep. D-33509*, Jet Propul. Lab., Calif. Inst. of Technol., Pasadena, Calif.

McHugh, M., M. Hervig, B. Magill, R. Thompson, E. Remsberg, J. Wrotny, and J. Russell (2003), Improved mesospheric temperature, water vapor and polar mesospheric cloud extinctions from HALOE, *Geophys. Res. Lett.*, *30*(8), 1440, doi:10.1029/2002GL016859.

McHugh, M., B. Magill, K. Walker, C. Boone, P. Bernath, and J. Russell III (2005), Comparison of atmospheric retrievals from ACE and HALOE, *Geophys. Res. Lett.*, *32*, L15S10, doi:10.1029/2005GL022403.

Miller, M., and A. Untch (2005), The new ECMWF high resolution forecasting system, paper presented at ECMWF Tenth Workshop on Meteorological Operational Systems, Eur. Cent. for Medium-range Weather Forecasting, Reading, UK.

Mlynczak, M., and J. Russell (1995), An overview of the SABER experiment for the TIMED mission, *Opt. Remote Sens. Atmos. 2*, NASA Langley Res. Cent., Langley, Va.

Pagano, T., H. Aumann, D. Hagan, and K. Overoye (2003), Prelaunch and in-flight radiometric calibration of the Atmospheric Infrared Sounder (AIRS), *IEEE Trans. Geosci. Remote Sens.*, *41*, 265–273.

Read, W. G., Z. Shippony, M. J. Schwartz, N. J. Livesey, and W. V. Snyder (2006), The clear-sky unpolarized forward model for the EOS Microwave Limb Sounder (MLS), *IEEE Trans. Geosci. Remote Sens.*, *44*, 1367–1379.

Read, W. G., et al. (2007), Aura microwave limb sounder upper tropospheric and lower stratospheric $H_2O$ and relative humidity with respect to ice validation, *J. Geophys. Res.*, *112*, D24S35, doi:10.1029/2007JD008752.

Remsberg, E., et al. (2002), Comparisons of SABER temperature profiles with rocket, groundbased, and satellite measurements, *Eos Trans. AGU*, *83*(47), Fall Meet. Suppl., Abstract SA62B-0405.

Remsberg, E., G. Lingenfelser, V. Harvey, W. Grose, J. Russell III, M. Mlynczak, L. Gordley, and B. Marshall (2003), On the verification of the quality of SABER temperature, geopotential height, and wind fields by comparison with Met Office assimilated analyses, *J. Geophys. Res.*, *108*(D20), 4628, doi:10.1029/2003JD003720.

Rienecker, M., et al. (2007), The GEOS-5 data assimilation system: A documentation of GEOS-5.0, *TM-2005104606 VOL27*, NASA Goddard Space Flight Cent., Greenbelt, Md.

Rodgers, C. D. (2000), *Inverse Methods for Atmospheric Sounding: Theory and Practice*, World Sci., Hackensack, N. J.

Schoeberl, M. R., et al. (2006), Overview of the EOS Aura mission, *IEEE Trans. Geosci. Remote Sens.*, *44*, 1066–1074.

Schwartz, M., W. Read, and W. Snyder (2006), EOS MLS forward model polarized radiative transfer for Zeeman-split oxygen lines, *IEEE Trans. Geosci. Remote Sens.*, *44*, 1182–1191.

Simmons, A., M. Hortal, G. Kelly, A. McNally, A. Untch, and S. Uppala (2005), ECMWF analyses and forecasts of stratospheric winter polar vortex breakup: September 2002 in the Southern Hemisphere and related events, *J. Atmos. Sci.*, *62*, 668–689.

Stajner, I., C. Benson, H. Liu, S. Pawson, N. Brubaker, L. Chang, L. Riishojgaard, and R. Todling (2007), Ice polar stratospheric clouds detected from assimilation of Atmospheric Infrared Sounder data, *Geophys. Res. Lett.*, *34*, L16802, doi:10.1029/2007GL029415.

Susskind, J., C. Barnet, and J. Blaisdell (2003), Retrieval of atmospheric and surface parameters from AIRS/AMSU/HSB data in the presence of clouds, *IEEE Trans. Geosci. Remote Sens.*, *41*, 390–409.

Susskind, J., C. Barnet, J. Blaisdell, L. Iredell, F. Keita, L. Kouvaris, G. Molnar, and M. Chahine (2006), Accuracy of geophysical parameters derived from Atmospheric Infrared Sounder/Advanced Microwave Sounding Unit as a function of fractional cloud cover, *J. Geophys. Res.*, *111*, D09S17, doi:10.1029/2005JD006272.

Tobin, D. C., H. E. Revercomb, R. O. Knuteson, B. M. Lesht, L. L. Strow, S. E. Hannon, W. F. Feltz, L. A. Moy, E. J. Fetzer, and T. S. Cress (2006), Atmospheric Radiation Measurement site atmospheric state best estimates for Atmospheric Infrared Sounder temperature and water vapor retrieval validation, *J. Geophys. Res.*, *111*, D09S14, doi:10.1029/2005JD006103.

Waters, J. W., et al. (2006), The Earth Observing System Microwave Limb Sounder (EOS MLS) on the Aura satellite, *IEEE Trans. Geosci. Remote Sens.*, *44*, 1075–1092.

Wickert, J., et al. (2001), Atmosphere sounding by GPS radio occultation: First results from CHAMP, *Geophys. Res. Lett.*, *28*, 3263–3266.

Wickert, J., T. Schmidt, G. Beyerle, R. König, C. Reigber, and N. Jakowski (2004), The radio occultation experiment aboard CHAMP: Operational data analysis and validation of vertical atmospheric profiles, *J. Meteorol. Soc. Jpn.*, *82*, 381–395.

Wu, W., R. Purser, and D. Parrish (2002), Three-dimensional variational analysis with spatially inhomogeneous covariances, *Mon. Weather Rev.*, *130*, 2905–2916.

C. O. Ao, R. E. Cofield, W. H. Daffer, B. J. Drouin, E. J. Fetzer, L. Froidevaux, R. A. Fuller, R. F. Jarnot, J. H. Jiang, Y. B. Jiang, B. W. Knosp, A. Lambert, J.-L. F. Li, N. J. Livesey, G. L. Manney, W. G. Read, M. L. Santee, M. J. Schwartz (corresponding author), W. V. Snyder, P. C. Stek, R. P. Thurstans, P. A. Wagner, J. W. Waters, and D. L. Wu, Jet Propulsion Laboratory, Mail Stop 183–701, 4800 Oak Grove Drive, Pasadena, CA 91109, USA. (michael.j.schwartz@jpl.nasa.gov)

P. F. Bernath, Department of Chemistry, University of York, York YO10 5DD, UK.

C. D. Boone, Department of Chemistry, University of Waterloo, Waterloo, Ont, Canada N2L 3G1.

K. Krüger, Leibniz Institute for Marine Sciences, IFM-GEOMAR, Kiel University, D-24148 Kiel, Germany.

M. G. Mlynczak, NASA Langley Research Center, Hampton, VA 23681-2199, USA.

S. Pawson, NASA Goddard Space Flight Center, Global Modeling and Assimilation Office, Greenbelt, MD 20771, USA.

J. M. Russell III, Hampton University, Hampton, VA 23668, USA.

A. M. Tompkins, European Centre for Medium-range Weather Forecasts, Reading RG1 1NT, UK.

K. A. Walker, Department of Physics, University of Toronto, Toronto, Ont, Canada M5T 3M7.